Energy & Environmental Science

Accepted Manuscript

This is an *Accepted Manuscript*, which has been through the Royal Society of Chemistry peer review process and has been accepted for publication.

Accepted Manuscripts are published online shortly after acceptance, before technical editing, formatting and proof reading. Using this free service, authors can make their results available to the community, in citable form, before we publish the edited article. We will replace this *Accepted Manuscript* with the edited and formatted *Advance Article* as soon as it is available.

You can find more information about *Accepted Manuscripts* in the Information for Authors.

Please note that technical editing may introduce minor changes to the text and/or graphics, which may alter content. The journal's standard Terms & Conditions and the Ethical guidelines still apply. In no event shall the Royal Society of Chemistry be held responsible for any errors or omissions in this *Accepted Manuscript* or any consequences arising from the use of any information it contains.

ROYAL SOCIETY OF CHEMISTRY

www.rsc.org/ees

Energy & Environmental Science
CREATED USING THE RSC LaTeX PCCP ARTICLE TEMPLATE – SEE www.rsc.org/electronicfiles FOR DETAILS
ARTICLE TYPE
www. rsc.org/xxxxxx | XXXXXXXX

Material descriptors for predicting thermoelectric performance

Jun Yan[a], Prashun Gorai[a,b], Brenden Ortiz[a], Sam Miller[c], Scott A. Barnett[c], Thomas Mason[c], Vladan Stevanović[a,b], and Eric S. Toberer*[a,b]

Received Xth XXXXXXXXXX 20XX, Accepted Xth XXXXXXXXX 20XX
First published on the web Xth XXXXXXXXXX 200X
DOI: 10.1039/b000000x

In the context of materials design and high-throughput computational searches for new thermoelectric materials, the need to compute electron and phonon transport properties renders direct assessment of the thermoelectric figure of merit (zT) for large numbers of compounds untenable. Here we develop a semi-empirical approach rooted in first-principles calculations that allows relatively simple computational assessment of the intrinsic bulk material properties which govern zT. These include carrier mobility, effective mass, and lattice thermal conductivity, which combine to form a semi-empirical metric (descriptor) termed β_{SE}. We assess the predictive power of β_{SE} against a range of known thermoelectric materials, as well as demonstrate its use in high-throughput screening for promising candidate materials.

Introduction

The rational design and discovery of new thermoelectric materials is limited by the need to accurately predict both the electron and phonon transport properties entering the thermoelectric figure of merit (zT)[1–4]. While the desired properties inherent to good thermoelectric performance have been known for more than a century[5], the design problem concerning optimum material structures and chemical compositions remains elusive. To this end, recent efforts have used high-throughput computations, focusing exclusively on the ground-state electronic structure of known materials, to identify potential thermoelectric candidates.[6–8] Realization of novel thermoelectric materials could enable scalable solar-thermal electricity generation and a diverse range of applications involving waste heat capture or cogeneration[9–11].

To improve the large-scale computational screening and identification of materials, a computationally-addressable metric (descriptor) that quantifies the full potential of materials for thermoelectric performance, including both electron and phonon transport, is required. In this work, we propose and validate a semi-empirical approach that is based on first-principles calculations and offers a relatively simple computational assessment of the intrinsic bulk material properties which govern zT. Our approach offers a bridge between ab-initio calculations and experiments by deriving semi-empirical relations for quantities that are nearly inaccessible to high-throughput computations such as carrier mobilities and lattice thermal conductivity. These material properties combine to form a quantitative semi-empirical descriptor β_{SE}. We demonstrate here the efficacy of β_{SE} in both predicting known thermoelectric materials, including those that are not used in developing the empirical relations for β_{SE}, and in high-throughput screening for new candidate materials.

The basis for the β_{SE} descriptor emerges from the thermoelectric figure of merit, zT, which depends on the Seebeck coefficient (α), electrical conductivity (σ) and the electronic and lattice components of the thermal conductivity κ_e and κ_L

$$zT = \frac{\alpha^2 \sigma T}{\kappa_e + \kappa_L}. \quad (1)$$

Inspection of Eq. 1 reveals challenges associated with direct assessment of zT as it depends on both the electronic and vibrational properties, including scattering phenomena. Electronic correlations can further complicate the evaluation of electronic transport. As such, the search for new thermoelectric materials has traditionally been led by experiment and guided by a mixture of serendipity, intuition, and simple models.

The complexity of the problem is further compounded

† Electronic Supplementary Information (ESI) available: [details of any supplementary information available should be included here]. See DOI: 10.1039/b000000x/

[a] *Colorado School of Mines, Golden, CO, USA; E-mail: etoberer@mines.edu*
[b] *National Renewable Energy Laboratory, Golden, CO, USA.*
[c] *Northwestern University, Evanston, IL, USA.*

Energy & Environmental Science Accepted Manuscript

by the fact that known good thermoelectric materials span a diverse chemical phase space as shown in Figure 1, which depicts ∼40,000 known stoichiometric and crystalline solids from the Inorganic Crystal Structure Database[12] which possess anions from groups IV to VI. Two simple descriptors have been chosen to highlight this diversity: the extent of covalent character and the average atomic mass. Here, the covalent character is assessed via the standard deviation of the electronegativity of the constituent atoms. Known thermoelectric materials, such as PbTe, Bi_2Te_3, $Yb_{14}MnSb_{11}$ and $Mg_2Si_{1-x}Sn_x$, identified by colored symbols, are found throughout this space. The better thermoelectric materials (with $zT > 1$) are generally found in the predominantly covalentand heavy region of this plot. Figure 1 also highlights the enormous number of materials that have not been considered experimentally for thermoelectric performance. Many promising compounds remain to be discovered, preferably via efficient methods such as high-throughput computations. Alloys and metastable polymorphs offer further avenues for the discovery of new thermoelectric materials; such compounds have a particularly great need for computationally-driven searches due to their broad phase space.

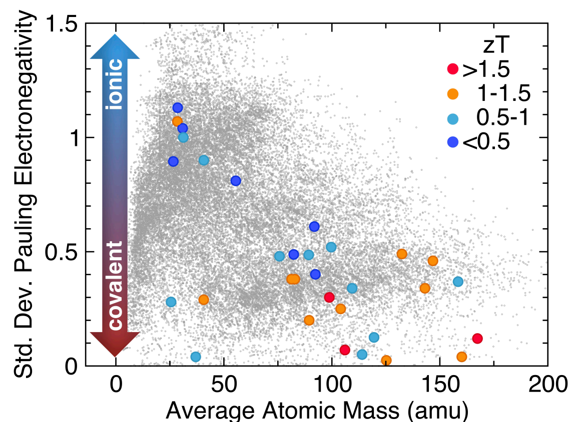

Fig. 1 Known compounds are extremely diverse, with a spectrum of electronegativity contrast and average atomic mass; thermoelectric materials (colored circles representing peak zT reported) have been discovered throughout this space. For clarity, only a subset of known thermoelectric compounds are shown.[20,26–59]

Approaches to thermoelectric discovery

With such a diverse phase space, the need for high-throughput computationally-driven searches for thermoelectric materials is critical. The first broad attempt to search beyond a single structural class was conducted by *Madsen*, who considered 570 antimonides[6]. This work analyzed the ground-state electronic structure employing the constant relaxation time approximation (CRTA) for solving the electronic Boltzmann transport equations.[13] As its name suggests, the CRTA treats the charge carrier relaxation time τ as an energy-independent term. In reality, an energy-dependent τ is expected for electron-phonon scattering; nevertheless, the CRTA approach is mathematically attractive as it enables one to obtain a reduced power factor ($\alpha^2\sigma/\tau$) as a function of chemical potential simply from the electronic band structure. Within this approach however, the ranking of different materials based on the reduced power factor requires that τ is not only constant for a given material, but also does not vary significantly from one material to the other. Furthermore, calculations of dopant levels, electron or phonon scattering and the phonon band structure were not included in this work due to their high computational cost. This work, however, succeeded in identifying n-type LiZnSb as a promising thermoelectric due to fairly high band degeneracy; our subsequent experimental efforts agreed with these calculations within the experimentally accessible doping range[14].

An alternative approach to addressing the scattering challenge has been proposed by *Curtarolo* and coworkers, who investigated ∼2,500 compounds.[8] The approach focuses on highly nanostructured materials by assuming that the bulk carrier mean free path is equal to or larger than the average grain size l. Therefore, if these structures are sufficiently fine-grained (∼5 nm), grain boundary scattering will dominate charge carrier scattering. Electronic structure calculations can then provide a performance metric given by $\alpha^2\sigma/l$. This metric can be used to compare predicted performance of different materials and sort promising candidates. Achieving high zT in this approach inherently requires large α, as the electronic mobility has been significantly reduced owing to enhanced grain boundary scattering.

On the other hand, rigorous calculations of electron-phonon scattering rates have been recently considered for simple materials (e.g. GaAs, GaP, Si, $Si_{1-x}Ge_x$) and were found to agree well with experiments[15–18]. Calculations of the vibrational properties and lattice thermal transport of individual materials have also seen significant advances[19–25]. However, these calculations, although of desired accuracy, are typically material-dependent and are sufficiently expensive that high-throughput searches are unlikely to adopt such methods in the near future for structurally complex materials.

In an attempt to develop a tractable computational approach taking into account both k_L and the energy-

This journal is © The Royal Society of Chemistry [year]
Energy & Environmental Science Accepted Manuscript

dependence of charge carrier scattering and that will allow screening of large, complex materials classes, we revisit simple descriptors for thermoelectric performance. Consideration of the Boltzmann transport equations within the relaxation time approximation yields an expression for zT,

$$zT = \frac{u\beta}{v\beta + 1}, \tag{2}$$

where u and v are functions that depend strictly on the chemical potential (η) and charge carrier scattering mechanism, and β is a material-dependent parameter that is independent of charge carrier chemical potential[60,61]. It is clear from inspection of Eq. 2 that large zT requires simultaneously maximizing β and optimizing η. β is defined as:

$$\beta = \left(\frac{k_B}{e}\right)^2 \frac{2e(k_BT)^{3/2}T}{(2\pi)^{3/2}\hbar^3} \frac{\mu_o m_{DOS}^{*3/2}}{\kappa_L} \tag{3}$$

where μ_o is the intrinsic charge carrier mobility and m^*_{DOS} is the density of states effective mass. In SI units, this expression simplifies to:

$$\beta = 5.745 \times 10^{-6} \frac{\mu_o \left(m^*_{DOS}/m_e\right)^{3/2}}{\kappa_L} T^{5/2} \tag{4}$$

Under the assumption that optimal η can be achieved, β is helpful in assessing the maximal zT achievable in a given material. In practice, most thermoelectric materials are optimized when η is close to the band edge, yielding an optimum carrier concentration near 10^{19}-10^{20} cm^{-3}.[62,63]

Predictive power of β

The efficacy of β in predicting zT can be assessed from prior experimental studies. We focus on compounds in which significant efforts have been undertaken to optimize carrier concentration, thus maximizing u/v and thereby zT for a given β. The magnitude of β is estimated from 300 K measurements, due to the dearth of high temperature mobility measurements in the literature. Further, if β_{300K} can be shown to be useful in predicting zT, such a result should be applicable to experimental screening of material libraries (e.g. spatially graded alloy films).[76,77]

In Fig. 2, we show a strong correlation between $\beta_{300K}^{1/2}$ at 300 K with the z corresponding to the the peak zT for 31 compounds.* The emphasis on z, rather than zT,

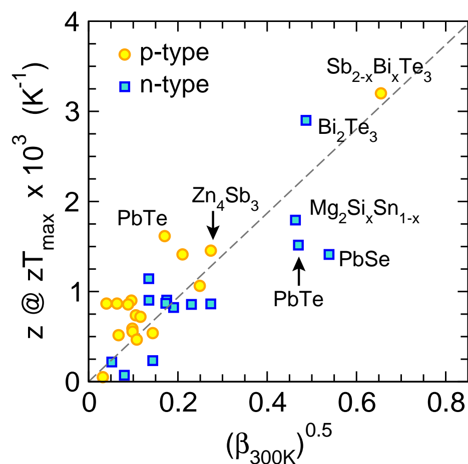

Fig. 2 Room temperature experimental measurements of β show a fairly good correlation with z at peak zT across a diverse range of compounds, despite differences in peak temperature. β_{300K} obtained using Eq. 4 and associated transport measurements from the literature.[26–50,54,64–75]

facilitates comparison of materials with different band gaps and peak temperatures. To achieve zT near unity at room temperature, thereby competing with Bi_2Te_3 for Peltier cooling applications, a z of ~0.003 K^{-1} is required. Achieving a zT of 3 at 1000 K would enable high efficiency solid state heat engines; again a z of ~0.003 K^{-1} is required. The similar T dependence of μ and κ_L and minimal T dependence of m^*_{DOS} helps maintain a fairly temperature-independent description of β. The material set considered is heavily weighted towards known thermoelectric materials, due to the requirement of carrier concentration optimization and high temperature property measurements. It is expected that most semiconductors will demonstrate experimental β that is far lower than the β values shown in Figure 2. It is important to note that a separate β can be defined for e^- and h^+ conduction. β values shown in Figure 2 correspond to the known carrier types for each of the compounds.

Semi-empirical description of β: Theory and model development

In the following section, we build the semi-empirical models for the room temperature μ_o and κ_L by combining standard DFT calculations, available experimental values (at 300 K) and classical scattering theory. These models serve to develop the semi-empirical approach to

* From solution to the Boltzmann transport equation within the relaxation time approximation (acoustic phonon-dominated), one finds that zT approximately scales as $\beta^{1/2}$ for a given temperature and an optimized η. Note that the optimum values for u and v depend on the magnitude of β and are adjusted via η.

Energy & Environmental Science Accepted Manuscript

β_{300K}, which we denote by $\beta_{\rm SE}$.

$$\beta_{\rm SE} \propto \frac{\mu_o \, (m^*_{DOS}/m_e)^{3/2}}{\kappa_L} \quad (5)$$

We also demonstrate that $\beta_{\rm SE}$ is equally predictive as β_{300K}, and can be used for *a priori* assessment of the potential of a material for thermoelectric applications, especially when critical parameters such as carrier mobility and thermal conductivity is not known.

Mobility

In the simplest approach to mobility, the charge carrier relaxation time (τ_e) is constant and $\mu_o = e\tau_e/m^*_b$, where m^*_b is the band effective mass. In this approximation, $\beta \propto m_b^{*1/2}$, suggesting that high band mass is desirable. However, a more nuanced view of τ_e finds that this proportionality is misleading.[78]

At room temperature and above, one would expect a combination of acoustic and optical phonons to dominate charge carrier scattering, which is consistent with the $\mu \propto T^{-1.5}$ observed experimentally at high temperature in thermoelectric materials and classic semiconductors.[26,45,47,79] Four distinct electron-phonon scattering mechanisms are known to be of importance in semiconductors: (i) acoustic deformation potential scattering (ii), optical deformation potential scattering (iii), polar optical phonon scattering, and (iv) piezoelectric scattering. Depending on the details of the electronic structure as well as of the phonon dispersion some of these mechanisms can contribute to both the intra- and the inter-valley scattering events. Because the piezoelectric scattering contributes at relatively low temperatures[79,80] we focus our discussion on the two deformation potentials and the polar optical phonon scattering mechanisms. These are, generally speaking, a consequence of the fact that phonons displace the ions in a crystal, thereby introducing changes in the dispersion of the electronic bands, which are described by the deformation potentials. In noncentrosymmetric crystals, phonons may also perturb the dipole moment between the atoms leading to a nonzero polarization of the material and induced fields. As such, the electron-phonon scattering mechanisms depend critically on the elastic properties of the material. For example, the following relation for the relaxation time associated with the acoustic deformation potential scattering can be shown to hold: $\tau \propto \frac{C_{ll}}{m_b^{*3/2}\Xi^2}$, where C_{ll} is the elastic constant for longitudinal vibrations and Ξ is the deformation potential of the relevant band edge. In addition, all of the discussed relaxation times depend inversely on the electronic DOS, which in the parabolic band approximation implies $(m^*_b)^{-3/2}$ dependence of τ on the band effective mass.

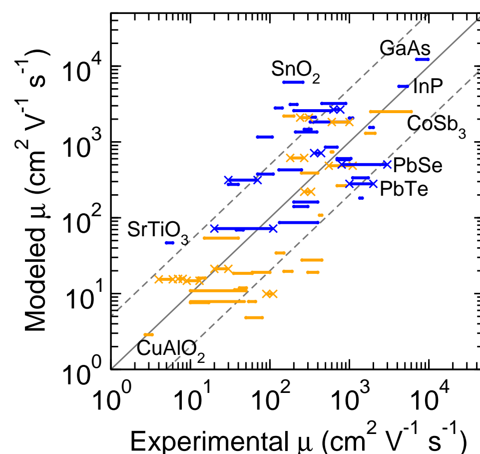

Fig. 3 The semi-empirical model of mobility is generally predictive within half an order of magnitude (dashed lines) from experimental values. Experimentally measured mobility values at 300K show a significant spread in the literature for any given material (single crystals are unmarked, polycrystalline ingots are denote with ×). Experimental mobility data (in orange for holes and in blue for electrons) are found in the Supplementary Information.

Motivated by these general features of the electron-phonon scattering mechanisms and taking into account the reciprocal additivity of the relaxation times (Matthiessen's Rule), we postulate the model for the carrier mobility as the combination of bulk modulus (B), describing the elastic properties of materials, and m^*_b in the following way:

$$\mu_o = A_o(B)^s(m^*_b)^{-t}, \quad (6)$$

where A_o, s and t are empirical parameters, which, as we show, provide a reasonable approximation for the mobility of band conductors (Eq. 6). The bulk modulus and m^*_b in Eq. 6 represent the DFT calculated values with band effective mass derived from the DOS effective mass and the band degeneracy (N_b) using $m_{DOS}^{*3/2} = N_b m_b^{*3/2}$. This expression for m^*_b is, strictly speaking, valid for symmetry-equivalent and isotropic (spherical) hole pockets/electron valleys.[61] However, these assumptions facilitate the calculations as they eliminate the need for fitting the curvature of the individual bands; rather, they simply require a sufficiently fine k-point mesh to (a) obtain the DOS and (b) accurately identify how many band extrema contribute to the band edge (See the methods section for the detailed description of the computational procedure). The band degeneracy algorithm was applied to 412 compounds to assess the effectiveness of determining

Energy & Environmental Science Accepted Manuscript

 This journal is © The Royal Society of Chemistry [year]

N_b across a broad range of compounds.

To test the validity of our model and to derive empirical values for A_o, s, and t, we performed an extensive literature survey for the measured values for the carrier mobilities for both holes and electrons. The Supplemental Information provides the values employed. The resulting experimental dataset is shown in Fig. 3, this comprises 31 materials from the literature including oxides, standard main-group semiconductors and other thermoelectric materials (full list provided in the supplementary section). The β parameter utilizes the intrinsic (non-degenerate) mobility μ_o; care was taken to determine μ_o from the literature when possible. This sample set is biased toward predominantly band conductor materials for two main reasons: (i) availability of experimental data and (ii) the hopping carrier transport implies heavy effective masses and potentially correlated electronic electronic behavior that is not well-described by β.

Electronic properties and bulk modulus were calculated for these 31 compounds to test our model. For these calculations, we only considered stoichiometric compounds; as such, only some of the materials from Fig. 2 are included in this "learning set". Figure 3 shows the experimentally measured carrier mobility at room temperature for our "learning set" of compounds against the modeled value using Eq. 6 with $s = 1$ and $t = 2.5$. The exponents s and t prove to be consistent with the classic scattering theories as discussed previously. The same prefactor, A_0, is used for both carrier types (h^+ and e^-). The experimental mobility for every material in Fig. 3 is represented with a horizontal line spanning the range of values that can be found in the literature. All the experimental values correspond to room temperature mobilities and special attention is paid to distinguish single crystal data from the mobilities measured in polycrystalline samples. As evident from Fig. 3 a very simple model defined by Eq. 6 is able to reproduce measured mobilities within a half an order of magnitude (dashed lines), which is typical of the deviation found in the experimental data. The band effective mass and the bulk modulus appearing in Eq. 6 are quantities readily accessible to the standard DFT calculations and at a relatively low computational cost, enabling a simple computational assessment of a quantity as complex as charge carrier mobility. By using a single scalar quantity such as bulk modulus to describe the elastic properties of materials, we were able to circumvent relatively complex and computationally costly calculations of the electron-phonon coupling constants. This allows a quantitative and computationally-tractable approach to predict carrier mobilities that can be applied efficiently in high-throughput screening.

Lattice thermal conductivity

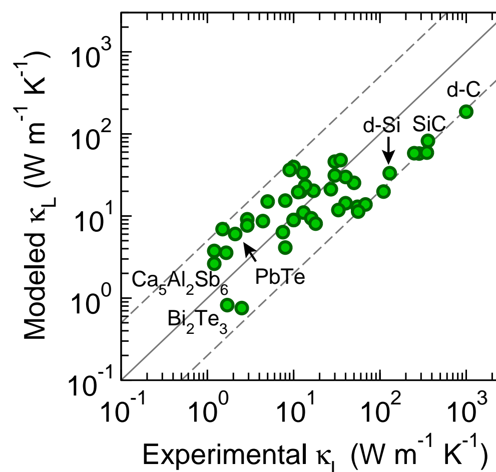

Fig. 4 Experimentally measured lattice thermal conductivities at 300 K can be predicted from ground-state DFT calculations and associated semi-empirical model. Dashed lines represent half an order of magnitude deviation from experimental values. Experimental κ_L data is found in the Supplementary Information.

We have previously shown[81] that κ_L can be modeled using simple descriptors for the acoustic and optical phonon modes. Specifically, with the known crystal structure data and experimental measurements of the speed of sound and Grüneisen parameter (γ), one can predict thermal conductivity within a factor of two for a broad range of compounds (e.g. d-Si to $Yb_{14}MnSb_{11}$; where the number of atoms in the primitive unit cell ranges from 2 to 104). We adopt a similar approach to derive an expression for κ_L using DFT calculations.

Acoustic phonons are generally the dominant modes within κ_L and can be approximated using a simplified Debye-Callaway model.[82] Using the high temperature limit for the heat capacity and the assumption that Umklapp scattering is the dominant scattering source, we have previously shown[81] the following expression can be obtained,

$$\kappa_{L,ac} = \frac{(6\pi^2)^{2/3}}{4\pi^2} \frac{\bar{M} v_s^3}{T V^{2/3} \gamma^2 n^{1/3}} \tag{7}$$

where $\bar{M}$ is the average atomic mass, V is the average volume per atom, v_s speed of sound, and n is the number of atoms in the primitive cell. The speed of sound depends on the bulk modulus B, shear modulus G and density. In this first iteration, we simply consider B and d and employ the approximation $v_s \simeq \sqrt{\frac{B}{d}}$. Values for

Energy & Environmental Science Accepted Manuscript

V, $\bar{M}$, and n can be obtained from the structural data associated with the compound.

The optical phonon modes cannot be entirely neglected, otherwise κ_L in complex, large n materials will asymptote to a null value and lead to an overestimation of β. Treating the optical modes using the minimum thermal conductivity limit, where the mean free path l is half a phonon wavelength[83], yields a minimum optical contribution at high temperature given by

$$\kappa_{L,op} = \frac{3k_b v_s}{2V^{2/3}} \left(\frac{\pi}{6}\right)^{1/3} \left(1 - \frac{1}{n^{2/3}}\right) \quad (8)$$

and can be considered in sum with $\kappa_{L,ac}$ to obtain κ_L. In the limit of n diverging to infinity (i.e. an amorphous material), one recovers a κ_L that is determined by v_s and V.

Together, $\kappa_{L,ac}$ and $\kappa_{L,op}$ provide a general expression for κ_L that can be obtained from ground-state calculations:

$$\kappa_L = A_1 \frac{\bar{M} v_s^3}{V^{2/3} n^{1/3}} + A_2 \frac{v_s}{V^{2/3}} \left(1 - \frac{1}{n^{2/3}}\right) \quad (9)$$

where A_1 and A_2 are fitted parameters. Here, γ has been incorporated into A_1 as a material-independent quantity. In practice, γ varies from approximately 0.5-3 in most materials and will contribute approximately an order of magnitude scatter to the modeled κ_L.

Figure 4 shows the predicted $\kappa_{L,ac} + \kappa_{L,op}$ against experimental measurements of 45 compounds. Experimental values were obtained from the literature and include nearly all compounds from Figure 3. Here, the only fitted parameters are the prefactors A_1 and A_2 (See Supplementary Information). The model is predictive within one order of magnitude across four orders of magnitude of experimental data. For comparison, we previously found Eq. 9 to be predictive within a factor of two if experimental values are used (including the Grüneisen parameter).[81]

β_{SE} predicts thermoelectric performance

In Figure 5 we demonstrate the predictive capability of β_{SE} through comparison with known thermoelectric materials that have experimentally optimized doping levels. Details of the β_{SE} calculation can be found in the Methods sections. Figure 5 shows that β_{SE} is predictive of the experimental z at the peak zT for optimally doped samples. Here, we have normalized the β_{SE} of each carrier type to PbTe for clarity. It is important to note that no predictions for any compounds are dramatically false-negative or false-positive. Furthermore, it can be seen that the DFT-based β_{SE} is nearly as predictive as the experimental β_{300K} shown in Figure 2. Further, the real power of β_{SE} is that it only requires relatively simple and computationally inexpensive density functional calculations. Such success provides a promising path forward for high throughput screening of known and hypothetical materials for their thermoelectric performance.

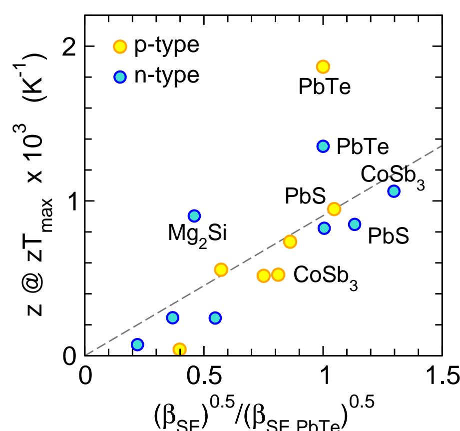

Fig. 5 β_{SE} calculated via DFT is a robust predictor of a material's intrinsic thermoelectric properties, here parameterized by the experimental z obtained at the peak zT. β_{SE} normalized to PbTe for comparison.

Next, we apply β_{SE} in exploring the potential of known materials from the ICSD database[12] for good thermoelectric performance. Figure 6 shows the scatter plot of 402 compounds (non-oxides) from the ICSD with 10 or less atoms in the primitive unit cell and a nonzero DFT/GGA band gap†. Each material is represented with a circle, the diameter of which is proportional to β_{SE}. The β_{SE} value is assessed against the carrier mobility (y-axis), lattice thermal conductivity (x-axis) and the band degeneracy (color code).

† In this study we include 10 oxide materials ranging from poorly conductive transition-metal oxides (CoO, Fe_2O_3, MnO, NiO, and VO_2) to main-group oxides which are known semiconductor materials (Bi_2O_3, Cu_2O, SnO_2, ZnO).

This journal is © The Royal Society of Chemistry [year]

Energy & Environmental Science Accepted Manuscript

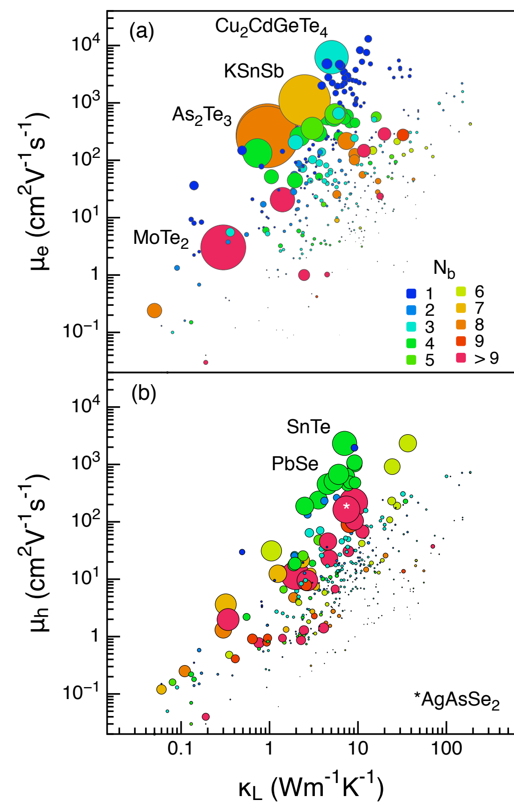

Fig. 6 Estimated β_{SE} for 412 semiconductors, represented via circle diameter for both (a) conduction and (b) valence band transport. Band degeneracy N_b increases across the color spectrum. In (a), PbS, PbSe, and PbTe are found in green below KSnSb. Source data can be found in the Supplementary Information.

Figure 6 finds good agreement between large β_{SE} and known thermoelectric compounds; the classic rock salt thermoelectric materials with high zT are well-represented (PbS, PbSe, PbTe). As expected, the majority of materials from our set appear to have relatively small β_{SE} value. Additionally, compounds which exhibit high β_{SE} are concentrated predominantly in the region with $\kappa_L \leq 10$ W m^{-1} K^{-1} and $\mu \geq 100$ cm^2 V^{-1} S^{-1} for both carrier types. Interestingly, the band degeneracy value is not strongly deterministic of ultimate β_{SE}. As is evident from Fig. 6, the fraction of compounds with simultaneously low β_{SE} value and relatively high N_b is quite large. Ultimately, β_{SE} requires the delicate balance of many inter-dependent material properties.

Another interesting feature of the data shown in Fig. 6 is that β_{SE} yields no cases which have both extremely low κ_L (below 1 W/mK) and high μ (above 100 cm^2/Vs). This is also true for the coexistence of relatively high κ_L (above 10 W/mK) and low μ (below 1 cm^2/Vs). This highlights the correlation between the electron-phonon and phonon-phonon scattering rates existing within the considered set of materials‡. The correlation follows from the classic scattering theory that we used to develop our approach, outlined in the previous sections. For systems with relatively small number of atoms in a unit cell, low κ_L typically arises from relatively low speeds of sound, which is a typical feature of low bulk modulus (i.e. soft) systems. From Eq. 6 it follows that soft systems are prone to having low carrier mobilities. Therefore, the analysis based on the β_{SE} descriptor indicates the existence of an optimal range for B that appears to be particularly suitable for good thermoelectric performance.

This initial exploration of the ICSD material space suggests several other compounds that may be worth further investigation. For example, $Cu_2CdGeTe_4$ and KSnSb (Figure 6a) are valence precise semiconductors where a combination of low m^* and low B leads to the potential for high thermoelectric performance if they can be rendered n-type. Recently, p-type $Cu_2CdSnSe_4$ and related alloys have exhibited peak zTs approaching unity; n-type β_{SE} of $Cu_2CdGeTe_4$ is a factor of 10 higher than the corresponding p-type β_{SE}, suggesting n-type doping is worth pursuing. The Zintl compound [84] KSnSb possesses polyanionic layers separated by K^+ ions; here the isotropic assumption of β_{SE} may coarsely approximate the behavior of a polycrystalline sample. High band degeneracy in $AgAsSe_2$ (Figure 6b) and $AgBiTe_2$ is also found to yield large β_{SE} values. These compounds have an ordered rock salt structure and are similar to $AgSbTe_2$, a component of the thermoelectric alloy TAGS (GeTe-$AgSbTe_2$).

Testing β_{SE}: Case studies

To highlight the key features and challenges with β_{SE}, we next turn our discussion to the properties of known thermoelectric materials: PbTe and Mg_2Si from our learning set, two SnSe phases ($Pnma$ and $CmCm$), and Sr_3GaSb_3. All of these compounds are known to be reasonably good thermoelectric materials [20,43,85], with the $Cmcm$ phase of SnSe exhibiting particularly high zT. Consistent with these experimental observations, we find that all of these materials exhibit large β_{SE}.

‡ The restriction to small n in this set of compounds limits the role that complexity can play in decoupling κ_L and μ.

Energy & Environmental Science Accepted Manuscript

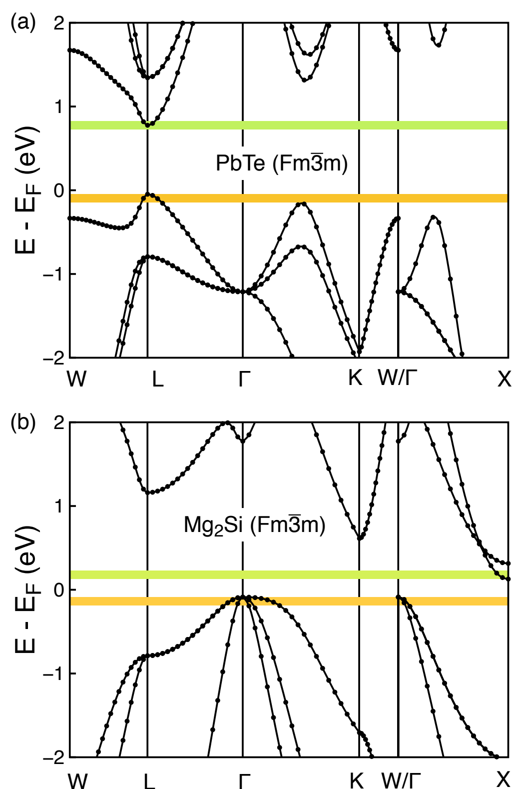

Fig. 7 Electronic band structures of (a) PbTe ($Fm\bar{3}m$), (b) Mg_2Si ($Fm\bar{3}m$). Energy window of 100 meV from the band edges are indicated by horizontal bars to highlight the band degeneracy.

PbTe: As a case study, PbTe provides an excellent example concerning the temperature dependence of electronic band structure, the role of band gap in these calculations, and the challenge associated with using a semi-empirical approach to assess the phonon scattering rate.

The DFT band structure of rocksalt PbTe is shown in Fig. 7a. Consistent with prior calculations, both band edges have extrema located at the L point, yielding an N_b of 4 from the band degeneracy algorithm.[86] Prior experimental work suggests that the band edges shift significantly at higher temperatures; this leads to the valence band extrema along $\Gamma - K$ contributing additional high-degeneracy conduction channels when optimally alloyed with Se on the Te site.[87,88] This improvement can be seen in Fig. 2, where 300 K experimental measurements underestimate the ultimate performance achievable in p-type PbTe at high temperature. Here, those extrema are just below the 100 meV energy window employed herein. To target materials with the potential for extremely large N_b, the energy window may be widened to account for temperature-dependent effects and the potential for the tuning of band energies through alloying. Neither temperature-induced changes in the band structure nor alloying can currently be addressed using high throughput first principles calculations; such developments would dramatically widen the phase space to which the β_{SE} approach could be applied.

The magnitude or character of the band gap (E_g) does not enter β_{SE}; this approach is thus insensitive to errors in E_g. The band gap, however, influences the dopability and the maximum temperature of good thermoelectric performance (limited by minority carrier activation and associated degradation in thermoelectric performance). In PbTe, the calculated E_g of 0.79 eV is overestimated compared to experiments due to the neglect of spin-orbit coupling in the calculation[89]. In the future, one could envision employing more accurate electronic structure methods such as many-body GW in combination with spin-orbit coupling[90] to better estimate a maximum achievable zT; such an approach could consider the minority and majority carrier transport properties (m^*_{DOS} and semi-empirical approximation of μ for each carrier type) and the magnitude of E_g.

It is well known that PbTe has extremely low κ_L (~2.3 W m^{-1} K^{-1} at 300 K); the sources for this has been attributed to: (i) the presence of soft, anharmonic bonding and heavy constituents, (ii) local symmetry breaking, and (iii) an unusual phonon dispersion that together lead to enhanced phonon-phonon coupling and Umklapp scattering opportunities.[33,91–94] The impact of these exotic scattering sources on the semi-empirical model's accuracy can thus be assessed.§ The resulting modeled κ_L is 6 W m^{-1} K^{-1}, higher than experiment due to the strong scattering in PbTe¶. Nevertheless, the difference is less than a factor of three in κ_L and suggests that the predictive power of β_{SE} is not precluded by variations in scattering rates.

Calculated values of β_{SE} predict that both n and p-type PbTe should be a good thermoelectric material, consistent with the existing literature[30–33,87]. For both carrier types, the source of this high zT arises from small m^*_b, medium N_b and low B and the ability to dope PbTe to the optimum compositions required to harness its large β.

Mg_2Si: As a case study, Mg_2Si highlights a broad challenge within high-throughput searches for thermoelectric materials: the role of dopants on the ultimate performance. Overall, good agreement between the semi-empirical and experimental values for μ_o, κ_L and B is

§ While PbTe was part of the κ_L learning set, it can be removed without changing the fit in coefficients A_1 and A_2.

¶ Good agreement between the calculated and experimental B of PbTe (38.3 and 39 GPa[95], respectively) suggests the phonon velocities are approximated reasonably well.

This journal is © The Royal Society of Chemistry [year]

Energy & Environmental Science Accepted Manuscript

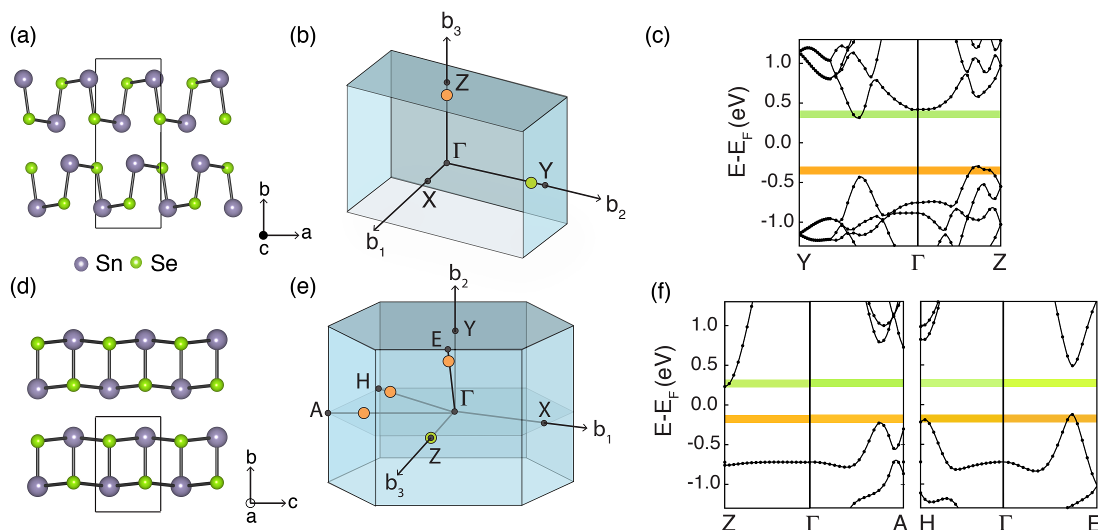

Fig. 8 Orthorhombic cells of SnSe with polymorph (a) *Pnma* and (d) *Cmcm*. The band extrema for the two structures are highlighted within the respective Brillouin zones using orange and green circles for valence and conduction band extrema, respectively. For clarity, the symmetry-equivalent extrema are not shown. The associated electronic band structures are shown in the region of the band extrema as well as the associated 100 meV window from the band edge.

found for Mg_2Si. However, Figure 5 shows that optimized Mg_2Si is a better thermoelectric material than predicted by β_{SE}. The source of this discrepancy arises from Bi doping on the Si site and the associated impact on transport properties. The above calculations and associated experimental comparison use the intrinsic semiconducting limit; however, optimized zT occurs at degenerate doping levels, which requires significant Bi doping. The large mass contrast associated with Bi doping lowers κ_L by approximately 25% without becoming a significant source of charge carrier scattering. Additionally, the electronic band structure of Mg_2Si (Fig. 7(b)) has nested conduction bands at X, with the upper band $\sim$250 meV above the band edge. Consistent with this band structure, analysis of the measured Seebeck coefficient using the single parabolic band model suggests a small increase in m^*_{DOS} both with increasing temperature and doping level[43]. However, the impact of this electronic effect on zT is small compared to the effect of Bi doping on phonon scattering rates. Mg_2Si highlights the challenge of studying heavily-doped semiconductors where dopant effects may be significant and potentially advantageous.[96]

SnSe: The high-temperature *CmCm* phase of SnSe, which is intrinsically p-type doped, has been reported to be a good TE material.[20] A high zT of $2.3 - 2.6$ is found along the shorter lattice vectors while a much lower zT of 0.8 is found along the longer crystal axis. The *Cmcm* phase transforms to the *Pnma* phase below $\sim$750 K, accompanied by a corresponding 50% decrease in the value of zT. The samples studied in Ref. [20], although p-type, were not intentionally doped, yielding extremely resistive samples where η was not optimized. We therefore focus on the individual transport properties rather than β_{SE}'s agreement with these experimental results.

Lattice thermal conductivities in the range 0.5-1.8 W m^{-1} K^{-1} were measured at 300 K; κ_L decreases gradually with increasing temperature. This broad range of values arises from the anisotropic transport inherent in SnSe. From the semi-empirical model developed above, we predict a κ_L of 2.8 W m^{-1} K^{-1} at 300K; this overestimation reflects the unusually high anharmonicity (and thus phonon-phonon scattering) found in SnSe compared to the materials utilized in the semi-empirical fit.

The band structure of both SnSe phases are plotted in Fig. 8, in agreement with previous calculations[20]. The high temperature phase has a band degeneracy of 8 and extremely light, parabolic valence band edge, with m^*_b of 0.08 m_e. In contrast, the low temperature phase has a more complicated valence band edge, highlighted in Fig. 8c. An anti-crossing between two bands along $\Gamma - Z$ has led to a highly non-parabolic band edge and significantly reduced carrier velocities. This low carrier velocity is captured in the algorithm employed herein; the large DOS near the band edge leads to a m^*_b of 0.4 m_e. The band degeneracy algorithm yielded a overall N_b of 2. In the prior experimental study of SnSe, a massive decrease in carrier mobility is observed upon the phase transition to the low temperature phase in these lightly-doped sam-

Energy & Environmental Science Accepted Manuscript

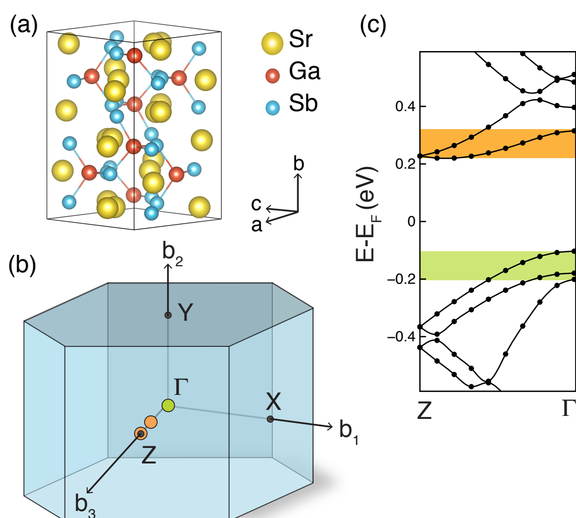

Fig. 9 a) Sr_3GaSb_3 is a Zintl compound built out of polyanionic $GaSb_3$ chains. The valence and conduction band maxima are shown (b) within the Brillouin zone as colored circles and (c) as a function of energy along $\Gamma - Z$ with 100 meV windows from the band edge highlighted by orange and green bars.

ples. Such a result is consistent with the anti-crossing inducing low carrier velocities in the room temperature phase and extremely light holes in the high temperature phase.

In concert, β_{SE} for the valence band edges of these two polymorphs is in good qualitative agreement with experiment, albeit neither phase has been optimized for carrier concentration. Consistent with experimental results, the *Cmcm* phase has a *p*-type β_{SE} which is twenty times greater than that of the *Pnma* phase (recall $zT \propto \sqrt{\beta}$ at a given temperature). The *n*-type β_{SE} of the *Pnma* phase is also quite large; this suggests excellent thermoelectric performance near room temperature potentially could be achieved if SnSe can be *n*-type doped. Both these cases of high β_{SE} are driven by very light m_b^* coupled with low κ_L and high band degeneracy in the case of the *Cmcm* phase.

Sr_3GaSb_3: While traditional thermoelectric materials have fairly simple structures (e.g. $Si_{1-x}Ge_x$, PbTe, Bi_2Te_3), many of the the recently discovered thermoelectric materials have dozens of atoms in their primitive cells.[26,42,68,72] It is therefore critical to consider the application of this semi-empirical model to complex semiconductors. One recent thermoelectric material is Sr_3GaSb_3, which has 56 atoms in its primitive cell and a complex polyanionic chain structure.[41] To date, Sr_3GaSb_3 has a maximum zT of 0.9 at 1000 K when *p*-type doped with Zn^{2+} on the Ga^{3+} site. The source of this high zT arises from the low κ_L, moderate μ, and fairly large m^*_{DOS} (1.2 W m^{-1} K^{-1}, 30 cm^2 V^{-1} s^{-1}, 0.9 m_e, respectively). With the 100 meV window utilized here, a valence band degeneracy of 3 is obtained, consistent with prior calculations. The calculated bulk modulus of 34 GPa is reasonably consistent with the experimental value of 39 GPa obtained from speed of sound measurements on polycrystalline disks.[41]

The valence band m^*_{DOS} is calculated to be 0.4 m_e from DOS parameterization; approximately half the value obtained through analysis of the experimental Seebeck coefficient. Using the semi-empirical approach to μ developed above, a room temperature value of 85 cm^2 V^{-1} s^{-1} is predicted for polycrystalline samples. Deviations from experiment can be attributed to (i) the reduced band mass compared to experiment and (ii) the observation of significant carrier activation in polycrystalline Sr_3GaSb_3 near room temperature. Extrapolating the high temperature, phonon-dominated mobility back to room temperature suggests a value of ∼60 cm^2 V^{-1} s^{-1} if a phase-pure sample could be obtained experimentally.

Concerning κ_L, the experimental result of 1.2 W m^{-1} K^{-1} is a factor of two smaller than the semi-empirical value. A reduced κ_L may result from secondary contamination, as observed in the μ measurements. Additionally, the mode Grüneisen parameter in such complicated structures may be larger than the average value in the learning dataset. In concert, the semi-empirical model predicts transport properties for Sr_3GaSb_3 that are in good agreement with experimental measurements; such results bode well for initial estimations of the thermoelectric performance of complex materials.

Conclusions

As we expand our search for thermoelectric materials to complex systems with dozens of atoms in the unit cell, we reach the edge of chemical intuition. This is particularly true for properties that emerge from reciprocal space, such as electronic and phonon structure and scattering phenomena. The development of a computationally tractable model of thermoelectric performance that takes into account both the electronic structure properties and the lattice thermal conductivity is thus essential for high-throughput computational screening of materials.

We have herein developed such a model using classical transport theory. To overcome the computationally expensive electron and phonon scattering rates required to predict zT, experimental data have been used to develop a semi-empirical model that only requires ground-

This journal is © The Royal Society of Chemistry [year]

Energy & Environmental Science Accepted Manuscript

state calculations. The efficacy of this model was assessed against known thermoelectric materials and was found to be predictive of z_{peak} within a factor of approximately two. The success of this model suggests the potential for high-throughput down-selection from within collections of materials using this ground-state approach. Such down-selection is critical for focusing computational and experimental resources on the most promising materials.

Acknowledgments

We acknowledge support from the NSF DMR program, Grant No. 1334713 and 1333335. The use of NREL's computing resources is gratefully acknowledged.

Methods

Electronic structure: DFT calculations are performed using the VASP code[97], in the generalized gradient approximation of Perdew-Burke-Ernzerhof (PBE)[98] within the projector augmented wave (PAW) formalism.[99] For the initial volume, cell shape and atomic relaxations we employed similar numerical approach (pseudopotentials, cutoffs, k-point mesh) as the one described in more detail in Ref. 100. The electrostatic Hubbard U correction is applied in cases where transition elements are present. The rotationally-invariant approach to the DFT+U introduced by Dudarev et al. is adopted.[101]

Spin degrees of freedom were treated explicitly for structures containing transition metal elements. For each material containing magnetic elements, we performed a limited search for the ground state magnetic configuration on a primitive unit cell initializing magnetic moments in five different ways: the non-spin-polarized, two ferro-magnetic initialization with low and high spin values, two additional calculations with random initialization of the spin orientations again starting from low and high spin values. The lowest energy spin configuration was selected as a representative for computing electronic structure properties of interest.

For the subsequent DOS, band degeneracy, and the effective mass calculation, the plane-wave cutoff is increased from 340 eV to 420 eV. The number of k-points are increased in a way that satisfies the relation $N_{atoms} \times N_{kpts} = 8000$, where N_{atoms} is the number of atoms in simulation cell and N_{kpts} is the number of k-points employed.[99] In this way sufficiently dense k-point grids are constructed that are compatible between different materials and are equivalent to the $16 \times 16 \times 16$ for diamond Si. Additionally, the bulk modulus is calculated by employing a standard fitting procedure of the Birch-Murnaghan equation of state to a set of total energies computed at different volumes near the minimum volume.[102,103]

DOS effective mass: The DOS effective mass is computed by fitting the m^*_{DOS} value in the standard equation for the density of states of the parabolic band

$$DOS(E) = \frac{1}{2\pi^2}\left(\frac{2m^*_{DOS}}{\hbar^2}\right)^{3/2} E^{1/2} \tag{10}$$

For calculating the band degeneracy (described below), the fit is done such that the parabolic DOS from Eq. 10 reproduces the number of states of the DFT-calculated DOS within a 100 meV energy window from the valence and conduction band edges. The DOS effective masses calculated in this way typically underestimate the masses measured in standard semiconductors with a uniform 0.6 exponent following from our extensive comparison with experimental data for values smaller than one. This correction has been applied throughout this work.

Band degeneracy: It is important to note that the band extrema may not always occur at high-symmetry points or along the high-symmetry lines of the Brillouin zone. Band degeneracy should, therefore, be evaluated over the entire Brillouin zone, as is done here-in. We evaluate N_b by identifying the carrier pockets (Fermi surface pockets) inside the first Brillouin zone, for valence and conduction band separately, assuming the Fermi-Dirac tail leads to conduction from states within 100 meV from the band edge and summing up the number of individual bands inside each pocket. Special attention is payed to resolving the symmetry relations between the equivalent Brilloiuin pockets as well as to the k-points that appear at the zone boundaries. The number of individual bands inside a given pocket we evaluate by counting the local band extrema inside that pocket. In this way we were able to reproduce the band degeneracy for all semiconductors which are included in this study, and which have their band structures and hence their band degeneracy well established (e.g. d-Si, GaP, PbTe and others). Additional validation was achieved by detailed study of the electronic structure of non-traditional compounds from the 412 materials discussed above. With knowledge of N_b and m^*_{DOS}, an approximate and average band effective mass (m^*_b) can be estimated within the approximation that the band extreme are identical, isotropic parabolic bands as: $m^*_b = m^*_{DOS} N_b^{-2/3}$.

Energy & Environmental Science Accepted Manuscript

References

1 G. J. Snyder and E. S. Toberer, Nature Mater., 2008, **7**, 105 – 114.
2 C. J. Vineis, A. Shakouri, A. Majumdar and M. G. Kanatzidis, Adv. Mater., 2010, **22**, 3970–3980.
3 A. J. Minnich, M. S. Dresselhaus, Z. F. Ren and G. Chen, Energy Environ. Sci., 2009, **2**, 466–479.
4 S. Curtarolo, G. L. W. Hart, M. B. Nardelli, N. Mingo, S. Sanvito and O. Levy, Nature Mater., 2013, **12**, 191–201.
5 E. Altenkirch, Physikalische Zeitschrift, 1909, **10**, 560580.
6 G. K. H. Madsen, J. Am. Chem. Soc., 2006, **128**, 12140.
7 J. Yang, H. Li, T. Wu, W. Zhang, L. Chen and J. Yang, Adv. Funct. Mater., 2008, **18**, 2880.
8 S. Wang, Z. Wang, W. Setyawan, N. Mingo and S. Curtarolo, Phys. Rev. X, 2011, **1**, 021012.
9 L. Bell, Science, 2008, **321**, 1457–1461.
10 D. Kraemer, B. Poudel, H. P. Feng, J. C. Caylor, B. Yu, X. Yan, Y. Ma, X. W. Wang, D. Z. Wang, A. Muto, K. McEnaney, M. Chiesa, Z. F. Ren and G. Chen, Nature Mater., 2011, **10**, 532–538.
11 L. L. Baranowski, G. J. Snyder and E. S. Toberer, Energy Environ. Sci., 2012, **5**, 9055–9067.
12 A. Belsky, M. Hellenbrandt, V. L. Karen and P. Luksch, Acta Crystallogr. B, 2002, **58**, 364.
13 G. K. H. Madsen and D. Singh, J. Comput. Phys. Commun., 2006, **175**, 67–71.
14 E. S. Toberer, A. F. May, C. J. Scanlon and G. J. Snyder, J. Appl. Phys., 2009, **105**, 063701.
15 J. Sjakste, N. Vast and V. Tyuterev, Phys. Rev. Lett., 2007, **99**, 236405.
16 F. Murphy-Armando and S. Fahy, Phys. Rev. B, 2008, **78**, 035202.
17 O. D. Restrepo, K. Varga and S. T. Pantelides, Appl. Phys. Lett., 2009, **94**, 212103.
18 Z. Wang, S. Wang, S. Obukhov, N. Vast, J. Sjakste, V. Tyuterev and N. Mingo, Phys. Rev. B, 2011, **83**, 205208.
19 Y. Zhang, E. Skoug, J. Cain, V. Ozoliņš, D. Morelli and C. Wolverton, Phys. Rev. B, 2012, **85**, 054306.
20 L.-D. Zhao, S.-H. Lo, Y. Zhang, H. Sun, G. Tan, C. Uher, C. Wolverton, V. P. Dravid and M. G. Kanatzidis, Nature, 2014, **508**, 373–377.
21 Y. Zhang, V. Ozoliņš, D. Morelli and C. Wolverton, Chem. Mater., 2014, **26**, 3427–3435.
22 D. A. Broido, M. Malorny, G. Birner, N. Mingo and D. A. Stewart, Appl. Phys. Lett., 2007, **91**, 231922.
23 W. Li, L. Lindsay, D. A. Broido, D. A. Stewart and N. Mingo, Phys. Rev. B, 2012, **86**, 174307.
24 L. Lindsay, D. A. Broido and T. L. Reinecke, Phys. Rev. Lett., 2012, **109**, 095901.
25 J. Carrete, W. Li, N. Mingo, S. Wang and S. Curtarolo, Phys. Rev. X, 2014, **4**, 011019.
26 A. F. May, E. S. Toberer, A. Saramat and G. J. Snyder, Phys. Rev. B, 2009, **80**, 125205.
27 X. Shi, Y. Pei, G. J. Snyder and L. Chen, Energy & Environ. Sci., 2011, **4**, 4086–4095.
28 Y. Wang, Y. Sui, J. Cheng, X. Wang, W. Su, X. Liu and H. J. Fan, J. Phys. Chem. C, 2010, **114**, 5174–5181.
29 V. K. Zaitsev, M. I. Fedorov, E. A. Gurieva, I. S. Eremin, P. P. Konstantinov, A. Y. Samunin and M. V. Vedernikov, Phys. Rev. B, 2006, **74**, 045207.
30 Y. Pei, A. LaLonde, S. Iwanaga and G. J. Snyder, Energy Environ. Sci., 2011, **4**, 2085–2089.
31 Y. Pei, A. D. LaLonde, H. Wang and G. J. Snyder, Energy Environ. Sci., 2012, **5**, 7963–7969.
32 Y. Pei, Z. M. Gibbs, B. Balke, W. G. Zeier and G. J. Snyder, Adv. Energy Mater., 2014, 1614–6840.
33 A. D. LaLonde, Y. Pei and G. J. Snyder, Energy Environ. Sci., 2011, **4**, 2090–2096.
34 H. Wang, Y. Pei, A. D. LaLonde and G. J. Snyder, Proc. Nat. Acad. Sci., 2012, **109**, 9705–9709.
35 H. Wang, Y. Pei, A. D. LaLonde and G. J. Snyder, Adv. Mater., 2011, **23**, 1366–1370.
36 D. M. Rowe, CRC Handbook of Thermoelectrics, CRC Press, 1995.
37 C. B. Vining, J. Appl. Phys., 1991, **69**, 331–341.
38 S. I. Johnson, A. Zevalkink and G. J. Snyder, J. Mater. Chem. A, 2013, **1**, 4244–4249.
39 A. Zevalkink, J. Swallow and G. J. Snyder, Dalton Trans., 2013, **42**, 9713–9719.
40 C. Liu, L. Miao, D. Hu, R. Huang, C. A. J. Fisher, S. Tanemura and H. Gu, Phys. Rev. B, 2013, **88**, 205201.
41 A. Zevalkink, W. G. Zeier, G. Pomrehn, E. Schechtel, W. Tremel and G. J. Snyder, Energy & Environ. Sci., 2012, **5**, 9121–9128.
42 T. Caillat, J.-P. Fleurial and A. Borshchevsky, J. Phys. Chem. Solids, 1997, **58**, 1119–1125.
43 S. K. Bux, M. T. Yeung, E. S. Toberer, G. J. Snyder, R. B. Kaner and J.-P. Fleurial, J. Mater. Chem., 2011, **21**, 12259–12266.
44 E. S. Toberer, P. Rauwel, S. Gariel, J. Tafto and G. Jeffrey Snyder, J. Mater. Chem., 2010, **20**, 9877–9885.
45 E. S. Toberer, A. F. May, B. C. Melot, E. Flage-Larsen and G. J. Snyder, Dalton Trans., 2010, **39**, 1046–1054.
46 A. F. May, J.-P. Fleurial and G. J. Snyder, Phys. Rev. B, 2008, **78**, 125205.
47 E. S. Toberer, A. Zevalkink, N. Crisosto and G. J. Snyder, Adv. Funct. Mat., 2010, **20**, 4375–4380.
48 S. Chen, H. Wang, W. Wan and X. Huang, Adv. Appl. Ceram., 2013, **112**, 331–336.
49 J. Li, J. Sui, Y. Pei, C. Barreteau, D. Berardan, N. Dragoe, W. Cai, J. He and L.-D. Zhao, Energy Environ. Sci., 2012, **5**, 8543–8547.
50 E. Guilmeau, D. Bérardan, C. Simon, A. Maignan, B. Raveau, D. O. Ovono and F. Delorme, J. Appl. Phys., 2009, **106**, 053715–053715.
51 D.-Y. Chung, T. Hogan, P. Brazis, M. Rocci-Lane, C. Kannewurf, M. Bastea, C. Uher and M. G. Kanatzidis, Science, 2000, **287**, 1024–1027.
52 F. Gascoin, S. Ottensmann, D. Stark, S. M. Haïle and G. J. Snyder, Adv. Funct. Mater., 2005, **15**, 1860–1864.
53 G. S. Nolas, D. T. Morelli and T. M. Tritt, Ann. Rev. Mater. Sci., 1999, **29**, 89–116.
54 H. Xie, H. Wang, Y. Pei, C. Fu, X. Liu, G. J. Snyder, X. Zhao and T. Zhu, Adv. Func. Mater., 2013, **23**, 5123–5130.
55 K. Fujita, T. Mochida and K. Nakamura, Jpn. J. Appl. Phys., 2001, **40**, 4644.
56 K. Koumoto, I. Terasaki and R. Funahashi, MRS Bulletin, 2006, **31**, 206–210.
57 T. Tsubota, M. Ohtaki, K. Eguchi and H. Arai, J. Mater. Chem., 1997, **7**, 85–90.
58 M. Ohtaki, T. Tokunaga, K. Eguchi and H. Arai, Proc. ICT'97. Int. Conf. Thermoelectrics, 1997, pp. 224–227.
59 H. Kuriyama, M. Nohara, T. Sasagawa, K. Takubo, T. Mi-

Energy & Environmental Science Accepted Manuscript

This journal is © The Royal Society of Chemistry [year]

zokawa, K. Kimura and H. Takagi, Proc. ICT'06. 25th Int. Conf. Thermoelectrics, 2006, pp. 97–98.
60 H. J. Goldsmid and R. W. Douglas, Brit. J. Appl. Phys., 1954, **5**, 386.
61 R. P. Chasmar and R. Stratton, J. Electron. Control, 1959, **7**, 52–72.
62 H. Goldsmid, Thermoelectric Refrigeration, Temple Press Books LTD, London, 1964.
63 G. S. Nolas, J. Sharp and H. J. Goldsmid, Thermoelectrics Basic Principles and New Materials Developments, Springer-Verlag, Berlin, Heidelberg, 2001.
64 X. Y. Li, L. D. Chen, J. F. Fan, W. B. Zhang, T. Kawahara and T. Hirai, J. Appl. Phys., 2005, **98**, 083702.
65 Y. Nagamoto, K. Tanaka and T. Koyanagi, Proc. Int. Conf. Thermoelectrics, 1998, **17**, 302–305.
66 H. Wang, E. Schechtel, Y. Pei and G. J. Snyder, Adv. Energy Mater., 2013, **3**, 488–495.
67 L.-D. Zhao, J. He, S. Hao, C.-I. Wu, T. P. Hogan, C. Wolverton, V. P. Dravid and M. G. Kanatzidis, J. Amer. Chem. Soc., 2012, **134**, 16327–16336.
68 E. S. Toberer, C. A. Cox, S. R. Brown, T. Ikeda, A. F. May, S. M. Kauzlarich and G. J. Snyder, Adv. Funct. Mater., 2008, **18**, 2795.
69 M. Zhou, Z. M. Gibbs, H. Wang, Y. Han, C. Xin, L. Li and G. J. Snyder, Phys. Chem. Chem. Phys., 2014, **16**, 20741–20748.
70 A. Zevalkink, E. S. Toberer, T. Bleith, E. Flage-Larsen and G. J. Snyder, J. Appl. Phys., 2011, **110**, 013721.
71 A. Zevalkink, G. S. Pomrehn, S. Johnson, J. Swallow, Z. M. Gibbs and G. J. Snyder, Chem. Mater., 2012, **24**, 2091–2098.
72 A. Zevalkink, E. S. Toberer, W. Zeier, E. Flage-Larsen and G. J. Snyder, Energy Environ. Science, 2011, **4**, 510–518.
73 N. Wang, H. Chen, H. He, W. Norimatsu, M. Kusunoki and K. Koumoto, Sci. Rep., 2013, **3**, 3449.
74 C. Ruttanapun, A. Wichainchai, W. Prachamon, A. Yangthaisong, A. Charoenphakdee and T. Seetawan, J. Alloys Compd., 2011, **509**, 4588–4594.
75 L. Lukyanova, V. Kutasov and P. Konstantinov, Phys. Sol. St., 2008, **50**, 2237–2244.
76 M. Otani, N. D. Lowhorn, P. K. Schenck, W. Wong-Ng, M. L. Green, K. Itaka and H. Koinuma, Appl. Phys. Lett., 2007, **91**, 132102.
77 R. Potyrailo, K. Rajan, K. Stoewe, I. Takeuchi, B. Chisholm and H. Lam, ACS Combi. Sci., 2011, **13**, 579–633.
78 C. Wood, Rep. Prog. Phys., 1988, **51**, 459–539.
79 Y. Y. Peter and M. Cardona, Fundamentals of Semiconductors, Springer-Verlag, Berlin, 3rd edn., 2005.
80 M. Lundstrom, Fundamentals of Carrier Transport, Cambridge university Press, Cambridge, 2000.
81 E. S. Toberer, A. Zevalkink and G. J. Snyder, J. Mater. Chem., 2011, **21**, 15843–15852.
82 J. Callaway, Phys. Rev., 1959, **113**, 1046–1051.
83 D. G. Cahill, S. K. Watson and R. O. Pohl, Phys. Rev. B, 1992, **46**, 6131–6140.
84 E. S. Toberer, A. F. May and G. J. Snyder, Chem. Mater., 2010, **22**, 624–634.
85 A. Zevalkink, W. G. Zeier, G. Pomrehn, E. Schechtel, W. Tremel and G. J. Snyder, Energy Environ. Sci., 2012, **5**, 9121–9128.
86 X. Chen, D. Parker and D. J. Singh, Sci. Rep., 2013, **3**, 3168.
87 Y. Pei, X. Shi, A. LaLonde, H. Wang, L. Chen and G. J. Snyder, Nature, 2011, **473**, 66–69.
88 Z. M. Gibbs, H. Kim, H. Wang, R. L. White, F. Drymiotis, M. Kaviany and G. Jeffrey Snyder, Applied Physics Letters, 2013, **103**, 262109.
89 L. Xu, Y. Zheng and J.-C. Zheng, Phys. Rev. B, 2010, **82**, 195102.
90 J. Vidal and X. Zhang and V. Stevanović and J.-W. Luo and A. Zunger, Phys. Rev. B, 2012, **86**, 075316.
91 O. Delaire, J. Ma, K. Marty, A. F. May, M. A. McGuire, M.-H. Du, D. J. Singh, A. Podlesnyak, G. Ehlers, M. Lumsden and B. C. Sales, Nature Mater., 2011, **10**, 614–619.
92 K. M. O. Jensen, E. S. Božin, C. D. Malliakas, M. B. Stone, M. D. Lumsden, M. G. Kanatzidis, S. M. Shapiro and S. J. L. Billinge, Phys. Rev. B, 2012, **86**, 085313.
93 E. S. Bozin, C. D. Malliakas, P. Souvatzis, T. Proffen, N. A. Spaldin, M. G. Kanatzidis and S. J. L. Billinge, Science, 2010, **330**, 1660–1663.
94 T. Keiber, F. Bridges and B. C. Sales, Phys. Rev. Lett., 2013, **111**, 095504.
95 Non-Tetrahedrally Bonded Elements and Binary Compounds I, ed. O. Madelung, U. Rssler and M. Schulz, Springer Berlin Heidelberg, 1998, vol. 41C, pp. 1–4.
96 J. P. Heremans, V. Jovovic, E. S. Toberer, A. Saramat, K. Kurosaki, A. Charoenphakdee, S. Yamanaka and G. J. Snyder, Science, 2008, **321**, 554–557.
97 G. Kresse and J. Furthmüller, Comput. Mater. Sci., 1996, **6**, 15.
98 J. P. Perdew, K. Burke and M. Ernzerhof, Phys. Rev. Lett., 1996, **77**, 3865–3868.
99 P. E. Blöchl, O. Jepsen and O. K. Andersen, Phys. Rev. B, 1994, **49**, 16223–16233.
100 V. Stevanović, S. Lany, X. Zhang and A. Zunger, Phys. Rev. B, 2012, **85**, 115104.
101 S. L. Dudarev, G. A. Botton, S. Y. Savrasov, C. J. Humphreys and A. P. Sutton, Phys. Rev. B, 1998, **57**, 1505–1509.
102 F. Birch, Phys. Rev., 1947, **71**, 809–824.
103 F. D. Murnaghan, Proc. Nat. Acad. Sci., 1944, **30**, 244–247.

Energy & Environmental Science Accepted Manuscript

Broader impacts

There is currently an up swell of excitement concerning computational driven materials discovery and design. However, this excitement is tempered by the substantial computational expense of many of the most intriguing properties. In thermoelectric materials, modeling electron and phonon transport in structurally complex materials is daunting, particularly within a high-throughput methodology. The ability to have computation provide accurate guidance in the search for new thermoelectric materials would be revolutionary; current efforts are typically within a trial-and-error experimental modality. Initial efforts to assess thermoelectric performance in a high throughput manner have focused on the ground state electronic structure and not attempted to grapple with the significantly more computationally costly aspects of charge carrier scattering or thermal transport. In this report, we develop and demonstrate a high throughput search methodology that addresses both electron and phonon transport, including charge carrier scattering. A semi-empirical quantitative descriptor is developed that combines ground state calculations and available experimental data. Incorporation of experimental data leverages the predictive power of the descriptor and offers a route to avoid complicated calculations. Semi-empirical models offer an attractive paradigm for high-throughput computational screening and may be enabling into material arenas beyond thermoelectrics.

Energy & Environmental Science Accepted Manuscript

CREATED USING THE RSC LaTeX PCCP ARTICLE TEMPLATE – SEE www.rsc.org/electronicfiles FOR DETAILS

Coefficients for semi-empirical model

The semi-empirical models for charge carrier mobility and lattice thermal conductivity are based on a evolving set of experimental data and associated calculations. As such, the fitted terms (s, t, A_o, A_1, A_2) are likewise expected to change as the model improves. For the fits employed within this paper, the following terms are used when the material parameters are in SI units:

Variable	Value	Units
s	1	none
t	2.5	none
A_o	1.2×10^{-14}	m s^{-1} J^{-1} V^{-1} $m_o^{-2.5}$
A_1	2.7×10^{-4}	K^{-1}
A_2	1.5×10^{-23}	J K^{-1}

Table 1 Room temperature experimental mobility (μ) data from the literature, divided by carrier type (holes - h and electrons - e) and sample form factor (single crystalline or polycrystalline). Mobilities values are in units of cm^2 V^{-1} s^{-1}.

	μ_h^{exp}		μ_e^{exp}		
Compound	s.c.	poly	s. c.	poly	Ref.
AlN	14	-	300	-	1,2
AlSb	300-400	-	200-400	-	3–6
BP	25-400	-	30-40	-	7–9
d-C	1,600-2,100	-	1800-2000	-	10–13
Ca_3AlSb_3	-	20-30	-	-	14,15
$Ca_5In_2Sb_6$	-	9-13	-	-	16,17
CdS	10-48	-	210-390	-	18–21
CdSe	10-17	-	450-900	700	22–26
CdTe	60	-	1000-1100	-	27,28
$CoSb_3$	1850-6000	240-310	70-110	30-70	29–34
Cu_2O	50-80	-	-	-	35–37
$CuAlO_2$	3	-	-	-	38
Ga_2O_3	-	-	130	-	39
GaAs	253-450	-	7000-9750	-	40–44
GaP	120-150	-	130-250	-	45–49
InP	150-190	-	4200-5370	-	50–53
Mg_2Ge	100	-	200-300	-	54,55
Mg_2Si	35-60	5	130-400	20-110	56–62
PbS	590-620	180-270	500-700	400	63–67
PbSe	700-1000	550-1100	700-1045	800-3000	64,65,68–72
PbTe	700-900	270-330	1100-1730	1000-2000	64,65,73,73–76
Si	420-450	-	1350-1450	-	77–82
SiC (3C)	15-40	-	322-980	-	83–87
SnO_2	-	-	150-260	-	88
SnTe	200	600-1000	-	-	64,89,90
$SrTiO_3$	-	-	5.5	-	91
TiO_2*	-	-	42	-	92
ZnO	-	-	200	205	93,94
ZnS	40	-	70-110	-	95–97
ZnSe	10-50	-	200-600	-	98–104
ZnTe	46	100	340	-	105–107

*anatase

Energy & Environmental Science Accepted Manuscript

This journal is © The Royal Society of Chemistry [year]

Table 2 Experimental lattice thermal conductivity (κ_L) at room temperature from the literature.

Compound	κ_L [W/mK]	Ref.	Compound	κ_L [W/mK]	Ref.
Al_2O_3	35	108	InP	68	109,110
AlN	285	111	Li_2O	11	112
AlSb	56	110,113	Mg_2Ge	13	114
BaO	40	115	Mg_2Si	8	56,114
BeO	250	116	MgO	30	117
BP	350	110	MnO	10	118
d-C	1000	119	NiO	30	118
Ca_3AlSb_3	1.6	120	PbS	2.9	63,110
$Ca_5Al_2Sb_6$	1.2	15	PbTe	2.1	73,76,110
$Ca_5In_2Sb_6$	1.2	16	Sc_2O_3	17	121
CaO	30	122	Si	130	110,123
CdS	16	110	SiC (3C)	360	124
CdSe	4.4	110,125	SiO_2	8	108
CdTe	7.5	110,113	SnO_2	40	126
$CoSb_3$	10	127	SnTe	1.5	125,128
CoO	14	129	SrO	12	110
Cr_2O_3	13	130	$SrTiO_3$	8.5	131
Cu_2O	5	108,132	VO_2	3	133
$CuAlO_2$	13	134	ZnO	50	110
Fe_2O3	5	135	ZnS	27	110
Ga_2O_3	14	136	ZnSe	33	110,114
GaAs	45-55	110,137	ZnTe	18	110
GaP	110	138			

Energy & Environmental Science Accepted Manuscript

This journal is © The Royal Society of Chemistry [year]

Table 3 Material properties used to determine β_{SE} obtained from high-throughput DFT calculations and subsequent analysis. The parameters in the table below form the basis of Figure 6 in the manuscript. The parameters include: chemical formulae, identification number from the Inorganic Crystal Structure Database (ICSD), number of atoms in the primitive unit cell (n), mass density (d) in g cm^{-3}, band gap (E_g) in eV, bulk modulus (B) in GPa, valence and conduction band degeneracies (N_V and N_C), and valence and conduction band DOS effective masses ($m^*_{DOS,V}$ and $m^*_{DOS,C}$) in the units of m_o. The origin of non-integer values for band degeneracies is in explicit treatment of the spin degrees of freedom and averaging over the two spin channels.

Compound	ICSD No.	SG No.	n	d	E_g	B	N_V	N_C	$m^*_{DOS,V}$	$m^*_{DOS,C}$
AsGa	067773	186	4	5.06	0.20	60.17	2	1	0.717	0.009
AsGa	610541	216	2	5.06	0.19	60.31	3	1	0.929	0.007
$AsKLi_2$	078938	59	8	2.23	0.71	19.35	1	1	0.976	0.086
As_2Mn_2Ba	041794	139	5	5.34	0.54	43.68	2	2	2.100	0.406
AsS_2Li	419061	9	8	3.01	1.06	21.98	10	2	1.618	1.218
$AsSe_2Cu$	042884	160	4	5.00	0.45	39.38	4	8	1.393	1.306
AgCl	056542	11	4	5.45	1.84	38.82	8	1	5.669	0.097
AgCl	056545	63	4	5.45	1.84	38.87	8	1	5.693	0.096
AgCl	056538	225	2	5.45	1.84	37.65	8	1	6.286	0.125
Al_2O_3	161062	63	10	4.02	4.25	181.78	1	1	1.647	0.094
Al_2O_3	169722	13	10	3.87	5.87	230.31	3	1	7.765	0.111
Al_2O_3	173014	1	10	2.88	1.86	96.20	3	1	6.435	1.661
Al_2O_3	082504	12	10	3.51	4.45	183.17	3	1	3.681	0.110
Al_2O_3	151589	167	10	3.87	5.87	230.30	3	1	7.808	0.116
AsMnRb	610910	129	6	4.20	0.87	16.48	2	1	2.781	0.049
$AsSe_2Ag$	020087	166	4	6.42	0.07	59.08	12	1	0.535	0.061
As_2Te_3	068110	166	5	5.91	0.36	11.66	2	8	1.462	0.119
As_2Te_3	041040	160	5	5.90	0.37	11.56	2	8	1.459	0.124
As_2Te_3	030981	12	10	5.78	0.44	10.65	2	4	2.240	0.114
$AsLi_3$	610783	194	8	2.46	0.69	34.92	2	2	1.299	0.366
As_2PtRb_2	107529	63	10	5.38	0.87	17.54	5	2	5.615	0.810
AsMnLi	060742	129	6	3.95	1.02	43.40	3	2	1.910	0.655
$AsSe_2Li$	248118	1	8	4.46	0.32	21.69	8	2	1.429	0.418
$AsSe_2Li$	248116	9	8	4.37	0.78	19.47	8	2	2.477	1.786
BrCu	024770	186	4	5.08	1.47	38.31	3	1	2.309	0.073
BrCu	078274	216	2	5.09	1.44	38.65	3	1	2.913	0.083
BrCu	078280	225	2	6.08	1.20	47.19	2	1	5.716	0.059
Br_6SnRb_2	158956	225	9	3.85	1.31	9.08	11	1	6.185	0.304
BeSbLi	100114	186	6	4.47	0.87	56.23	3	3	0.299	0.851
BN	162876	62	8	3.03	5.65	285.19	3	2	1.474	1.163
BN	162877	8	8	2.27	1.56	173.22	7	1	4.157	1.152
BN	183257	186	4	3.44	5.23	373.07	2	2	0.899	0.168
BN	614864	216	2	3.45	4.47	373.09	3	3	1.149	0.256
BN	162875	136	8	3.30	4.84	348.29	3	2	1.818	0.233
BN	182731	1	2	3.45	4.47	373.18	3	3	1.085	0.194
BN	162882	9	8	2.54	3.38	93.94	6	2	2.999	1.119
BrAg	056547	225	2	6.30	1.47	34.60	2	1	5.798	0.080
BrAg	056550	11	4	6.30	1.46	35.01	4	1	5.130	0.061
BeLiP	042037	129	6	1.99	1.15	62.31	3	1	1.190	0.166
BeK_4As_2	300111	166	7	2.14	0.90	15.84	20	1	12.415	0.150
BeAsLi	609869	129	6	3.45	0.99	53.62	3	1	0.978	0.209
Bi_2O_3	168810	160	10	8.04	2.34	19.28	1	1	11.428	1.831

Energy & Environmental Science Accepted Manuscript

Compound	ICSD No.	SG No.	n	d	E_g	B	N_V	N_C	$m^*_{DOS,V}$	$m^*_{DOS,C}$
Bi_2O_3	027150	224	10	8.64	1.45	14.74	2	1	2.641	0.411
B_6Ba	612527	221	7	4.29	0.05	144.34	6	6	0.669	0.620
BBi	184569	216	2	8.73	0.24	72.37	3	1	0.465	0.011
Br_3Ti	039784	2	8	3.52	1.74	1.76	4	1	5.458	5.775
C_3Al_4	052287	166	7	2.93	1.33	159.06	2	3	3.366	0.423
C_3Al_4	014397	160	7	2.93	1.33	159.11	2	3	3.186	0.327
Ca_3BN_3	095814	123	7	2.77	0.53	80.32	2	1	1.905	0.157
CuBr	024770	186	4	5.08	1.47	38.31	3	1	2.309	0.073
CuBr	078274	216	2	5.09	1.44	38.65	3	1	2.913	0.083
CuBr	078280	225	2	6.08	1.20	47.19	2	1	5.716	0.059
$CrSe_2Na$	042392	166	4	4.48	0.55	44.87	1	1.5	1.519	0.648
CrS_2Ag	604981	160	4	4.88	0.84	67.87	1	1.5	1.486	0.559
Cr_2S_3	016721	148	10	3.64	0.59	63.00	1.5	0.5	0.837	0.787
C_2Ba	056160	139	3	3.79	1.57	39.61	6	2	13.347	0.677
Cr_2MnSe_4	626299	12	7	5.31	0.29	50.66	3.5	2	0.601	0.323
CoO	043458	186	4	5.10	1.10	127.25	2	1	4.536	0.141
CrS_2Li	150675	150	4	3.14	1.20	59.12	1.5	1.5	3.492	1.747
CrS_2Li	026233	164	4	3.14	1.20	59.12	1.5	1.5	3.496	1.761
Cr_2S_4Mn	626279	12	7	3.69	0.91	62.71	2.5	1.5	0.939	1.869
CrS_2Ba	165626	59	8	4.17	0.55	49.45	1	1	1.002	1.301
C_2AuLi	411253	187	4	5.62	1.68	23.43	4	3	3.012	0.238
$CrSi_2$	096026	181	9	4.99	0.65	190.78	2.5	1.5	0.908	1.270
$CrSi_2$	626787	180	9	4.99	0.62	94.34	2.5	1.5	0.756	1.161
Cr_2S_4V	081891	12	7	3.72	0.49	66.12	1.5	2	0.899	1.964
Cr_2FeSe_4	625968	12	7	5.45	0.19	57.83	3.5	1.5	0.619	1.191
C	182761	139	4	3.30	2.58	399.70	2	2	0.365	0.454
C	066464	227	2	3.49	4.15	432.43	3	6	0.360	0.804
C	182760	12	8	3.33	3.49	399.94	1	1	0.182	0.243
C	027422	194	4	3.48	3.36	433.57	2	2	0.277	0.131
C	028859	227	2	3.49	4.15	432.44	3	6	0.360	0.804
C	088819	206	8	3.55	2.44	385.62	3	1	0.369	0.100
C	067787	216	2	3.49	4.15	432.43	3	6	0.356	0.812
CrS_2Cu	174547	146	4	4.41	0.41	82.49	1	1.5	1.137	1.138
$CoBr_2$	052364	164	3	4.33	1.91	1.23	1	0.5	4.239	13.135
Cr_2S_4Fe	625931	12	7	3.85	0.64	69.00	0.5	1.5	0.280	2.144
CZr	183162	216	2	4.95	0.35	141.67	5	8	5.331	2.048
CrSe	024792	186	4	5.19	0.83	43.22	1	4	0.418	3.082
CrSe	162899	129	4	4.46	0.28	5.09	2	1	3.195	0.308
Ca_3AsCl_3	036002	221	7	2.59	1.83	37.82	3	3	0.866	1.008
Cr_2Se_4V	076523	12	7	5.28	0.18	56.28	1.5	0.5	1.037	1.930
CrS_2Au	088852	160	4	6.46	0.74	62.62	1	0.5	0.841	0.991
CaC_2	074665	87	3	2.20	1.27	53.46	2	2	3.378	0.505
$CrSiTe_3$	626810	148	10	4.94	0.31	2.62	2	2	1.059	0.954
CSn	182365	216	2	6.62	0.65	122.28	3	1	1.271	0.019
$FeCl_3$	063329	148	8	2.47	1.82	2.10	16	12	23.006	21.665
FeSe	169280	62	8	5.88	0.89	65.48	2	2	0.395	1.948
Fe_2O_3	182842	167	10	5.15	1.78	189.03	9	4	6.039	18.662
Ge_3As_4	163833	111	7	5.11	0.16	47.02	2	2	1.823	0.237
$Ge_2Te_5As_2$	068112	164	9	6.05	0.38	12.03	2	2	3.003	0.305
$GeSe_4BaAg_2$	411405	23	8	5.55	0.27	33.98	3	1	0.310	0.036

Energy & Environmental Science Accepted Manuscript

This journal is © The Royal Society of Chemistry [year]

Compound	ICSD No.	SG No.	n	d	E_g	B	N_V	N_C	$m^*_{DOS,V}$	$m^*_{DOS,C}$
$GeAs_2Cd$	042098	122	8	5.28	0.08	52.44	2	1	0.763	0.020
GeC	182363	216	2	5.77	1.65	170.69	3	3	1.205	0.343
$GeCoS_4Cu_2$	099293	121	8	4.28	0.54	69.92	2	0.5	0.946	1.121
$GeSe_4Cu_2Cd$	619750	121	8	5.46	0.15	53.53	3	1	1.584	0.015
$GeSe_2$	090956	82	6	4.32	1.63	13.83	5	3	0.808	1.535
$GeSe_2$	050761	122	6	4.30	1.64	13.82	5	4	0.708	1.616
GeAlLi	170035	216	3	3.26	0.05	55.95	3	3	0.496	0.289
GeAlLi	152087	216	3	3.26	0.05	55.95	3	3	0.520	0.291
GeTe	655497	160	2	5.87	0.57	29.69	6	3	0.695	0.415
GeTe	659805	160	2	5.88	0.57	29.69	6	3	0.694	0.422
GeTe	638010	225	2	6.10	0.37	49.03	4	8	0.082	0.526
GeTe	638014	166	2	6.10	0.37	49.03	4	8	0.078	0.513
$GeTe_4Cu_2Cd$	656154	121	8	5.79	0.03	41.98	3	3	0.792	0.018
I_6SnRb_2	022104	225	9	4.20	0.10	8.02	9	1	4.501	0.128
IBr	022120	36	4	3.48	1.38	0.87	7	2	3.290	4.859
I_2Ni	022108	166	3	4.40	0.73	0.76	3	8	5.492	2.078
$IBiSe_2Cd$	171727	12	10	6.58	1.29	22.38	3	2	0.943	0.319
IIn	055183	63	4	5.21	1.32	11.10	6	4	0.404	0.220
I_2TePd	409062	2	8	5.87	0.68	5.25	7	1	1.137	1.351
$I_6Au_2Rb_2$	170791	12	10	4.98	0.74	5.50	6	1	4.065	1.491
I_2Sn	002831	12	9	4.99	1.75	7.69	4	2	1.412	0.509
I_4Ti	039820	15	10	3.99	1.37	1.03	3	4	3.672	9.902
ITeBi	074501	143	3	6.28	1.24	2.44	2	1	2.645	0.258
ITeBi	079364	156	3	6.27	1.24	2.75	2	1	2.675	0.256
ICu	060719	216	2	5.60	1.87	34.14	3	1	1.941	0.075
ICu	024772	186	4	5.59	1.91	33.99	3	1	1.613	0.063
ICu	080255	166	4	5.36	0.21	26.54	2	1	2.046	0.038
IAg	043435	221	2	6.78	0.34	29.58	2	1	7.645	0.028
IAg	161581	225	2	6.67	1.38	30.86	2	3	5.791	0.342
IAg	056557	11	4	6.66	1.37	30.73	4	3	5.081	0.248
IAg	063655	186	4	5.32	1.93	22.59	3	1	1.967	0.092
IAg	164963	216	2	5.32	1.90	22.32	3	1	2.274	0.106
IZrN	036119	59	6	4.73	1.83	0.74	1	1	0.720	0.770
$ISAg_3$	201004	221	5	6.41	0.96	39.06	12	1	1.817	0.048
$ISAg_3$	174095	146	5	6.57	0.91	30.67	6	1	7.266	0.039
I_4P_2	203216	2	6	3.39	1.93	1.07	5	3	2.485	2.508
ISbTe	035471	2	6	5.30	0.86	4.03	2	2	2.662	0.328
ISbTe	031355	12	6	5.28	0.86	4.04	2	1	2.708	0.322
$ISbMnSe_2$	281558	12	10	5.37	0.99	22.55	3	2	1.192	0.534
$I_2Br_4Rb_2Pd$	412835	139	9	4.29	0.69	11.36	3	1	3.704	0.269
K_2C_2Pt	421492	164	5	4.08	1.31	26.22	2	3	5.279	0.551
K_2TeBr_6	065118	225	9	3.46	1.98	10.02	3	4	5.671	0.860
K_2Br_4Pt	006063	123	7	3.95	1.98	10.25	2	1	7.190	1.004
KMnAs	060745	129	6	3.58	1.07	24.36	2	1	2.983	0.063
K_2S_2Pt	026258	71	5	4.53	1.59	32.65	8	4	6.908	2.748
$K_3As_2Ag_3$	032016	166	8	4.31	1.41	21.16	5	2	5.214	0.157
K_2CoSe_2	067390	72	10	3.28	1.97	21.48	16	21.5	10.122	14.627
$KFeSe_2$	632405	15	8	3.57	1.04	14.18	3	1	1.593	6.127
K_2BiAg	001156	20	8	4.49	0.71	14.91	2	1	4.023	0.054
K_2AsCu	043936	63	8	3.14	1.09	20.04	3	1	2.107	0.099

Energy & Environmental Science Accepted Manuscript

Compound	ICSD No.	SG No.	n	d	E_g	B	N_V	N_C	$m^*_{DOS,V}$	$m^*_{DOS,C}$
K_2SnBr_6	158955	225	9	3.54	1.21	10.32	9	1	5.845	0.244
KMnBi	601586	129	6	5.14	0.58	19.49	2	1	2.608	0.028
K_2Se_2Pt	040430	71	5	5.15	1.26	27.05	9	4	5.483	2.101
KSeCu	012157	194	6	4.04	0.60	30.70	4	1	1.285	0.047
K_2As_2Ge	071222	72	10	3.13	0.84	19.35	1	3	1.629	2.341
K_2As_2Pt	610762	63	10	4.88	0.67	19.46	2	2	3.316	0.723
K_2MnCl_6	009679	225	9	2.36	0.68	12.37	12	12.5	7.114	0.934
KSeAg	052586	129	6	4.68	0.83	25.62	2	1	2.723	0.052
$KNbSe_2$	026288	194	8	5.06	0.78	55.43	1	10	0.605	3.334
K_2AsAg	001154	20	8	3.54	1.06	19.33	3	1	3.337	0.106
K_2CoS_2	067387	72	10	2.53	2.08	25.36	10	9	6.328	16.323
K_2Br_6Pt	023771	225	9	4.28	1.10	11.35	9	3	5.548	0.846
K_2S_2Pd	641296	71	5	3.33	1.37	31.63	8	4	7.304	2.753
KTeCu	012158	194	6	4.32	0.92	24.37	4	1	0.972	0.050
K_2Br_4Pd	001982	123	7	3.36	1.60	10.15	3	1	5.876	1.219
K_2Te_2Pt	040432	71	5	5.28	0.91	21.24	2	4	1.887	1.626
Li_2ZrN_2	078790	164	5	4.19	1.88	125.62	2	3	0.903	2.301
$LiSe_2In$	056532	122	8	4.29	1.59	30.39	3	1	1.422	0.099
$LiSe_2In$	056531	166	4	5.26	0.83	39.69	11	3	3.929	0.470
MgAsLi	107954	216	3	2.95	1.37	46.68	3	3	1.822	0.340
$MnTe_4Al_2$	608538	121	7	4.48	0.90	26.93	2	1.5	1.106	0.187
Mo_2S_3	062486	11	10	4.91	0.93	39.21	6	3	2.867	2.332
$MgGeAs_2$	182368	122	8	4.02	0.57	52.02	1	1	0.341	0.018
$MoTe_2$	024155	194	6	6.87	0.97	5.23	8	18	2.447	2.403
Mg_2Si	150956	225	3	1.99	0.22	54.52	3	3	1.271	0.474
MgBiLi	108112	216	3	5.05	0.46	31.60	3	1	1.158	0.012
Mg_2Ge	165768	225	3	3.06	0.16	49.97	3	3	1.184	0.359
$MnSe_4Ga_2$	659100	121	7	4.66	0.65	33.82	2	0.5	1.137	0.042
MnSe	643584	225	2	5.27	0.33	66.71	1	1.5	2.742	0.133
MnSe	076218	194	4	5.39	1.46	63.61	2	6	0.650	3.640
MnSe	162900	129	4	4.04	2.18	1.52	8	2	3.243	1.764
MnSe	643594	186	4	4.17	1.77	47.06	2	1	2.540	0.095
MnO	028898	225	2	5.16	0.01	146.96	1	1.5	3.790	0.043
Na_2MgSn	000262	194	8	2.80	0.04	22.12	4	3	1.728	0.319
NiK_2As_2	300120	63	10	3.53	0.51	20.77	1	2	5.466	0.683
$NaSbLi_2$	054244	225	4	3.29	0.68	29.16	3	3	1.031	0.256
$NiSi_3P_4$	039452	121	8	3.15	0.35	104.08	2	4	0.623	0.979
Na_2C_2Pt	411389	164	5	4.76	0.68	32.35	3	3	2.658	0.191
NiSnZr	105382	216	3	6.78	0.03	87.16	3	8	4.126	2.079
NaS_2Fe	037026	23	8	2.16	1.52	17.95	5	27	4.765	15.004
Na_3Se_4Sb	065141	217	8	3.88	0.98	18.91	17	1	2.225	0.344
Na_2CuP	001153	63	8	2.94	0.97	33.27	1	1	0.647	0.265
NiO	076670	12	2	6.59	0.77	186.35	6	0.5	3.419	1.106
NiO	092132	166	2	6.59	0.77	186.32	6	0.5	3.414	1.108
NiO	076640	166	2	6.59	0.77	186.41	6	0.5	3.449	1.092
NiO	184626	225	2	6.59	0.77	186.32	6	0.5	3.422	1.104
$NaTe_2Cu_3$	060860	160	6	6.12	0.39	35.46	2	1	0.837	0.026
NiS_4Ga_2	634901	164	7	3.66	0.89	4.65	2	3.5	5.814	0.497
Na_2S_2Co	067386	72	10	2.68	1.78	32.65	6	15.5	3.461	15.264
$NiCN_2$	249388	194	8	4.06	1.48	104.16	2	2	1.249	5.957

Energy & Environmental Science Accepted Manuscript

This journal is © The Royal Society of Chemistry [year]

Compound	ICSD No.	SG No.	n	d	E_g	B	N_V	N_C	$m^*_{DOS,V}$	$m^*_{DOS,C}$
NiK_2P_2	300119	63	10	2.66	1.02	23.72	1	2	5.006	5.289
NaMnP	060728	129	6	3.03	1.11	40.74	2	2	2.789	1.653
$NaNbS_2$	026285	194	8	4.03	0.72	73.49	1	2	0.567	2.062
Na_2AsCu	043937	63	8	3.59	0.94	29.76	1	4	0.556	0.424
Na_2AsAg	049007	20	8	4.08	0.83	27.35	1	1	0.547	0.254
$NaAsK_2$	409224	194	8	2.19	0.17	15.38	4	1	3.803	0.030
NLi_3	034781	191	4	1.29	0.99	51.43	2	1	2.341	0.091
NLi_3	156899	194	8	1.65	1.29	64.78	2	2	2.739	0.414
NaAsMn	026461	129	6	3.88	1.00	35.62	2	3	2.480	0.337
$NbTe_4Cu_3$	628495	215	8	5.97	1.15	25.02	7	3	0.994	2.454
NiS	042493	186	4	5.33	0.48	97.38	2	12	1.133	3.284
NiS	042492	194	4	5.33	0.48	97.40	2	12	1.134	3.283
$NaNbSe_2$	026287	194	8	5.36	0.59	60.09	9	2	0.802	1.715
NiP_2	091560	15	6	4.52	0.62	87.14	2	6	0.760	0.560
NiP_2	027160	15	6	4.53	0.62	87.14	2	6	0.757	0.565
$NbSe_4Cu_3$	073956	215	8	5.19	1.65	28.58	7	3	1.530	2.418
NaAsBe	100091	194	6	3.09	1.31	37.94	4	7	1.251	2.329
OCu_2	173983	224	6	6.10	0.72	100.45	3	1	3.955	0.440
O_2V	089471	10	6	4.45	1.17	231.66	8	2	6.325	1.576
O_2V	034421	136	6	4.45	1.17	231.64	5	2	6.328	1.583
PMnLi	026458	129	6	2.97	1.02	49.44	3	2	2.018	0.589
PIn	024517	216	2	4.60	0.48	59.43	3	1	1.179	0.013
PIn	180911	186	4	4.59	0.54	59.15	3	1	0.987	0.012
PbTe	153710	62	8	7.91	0.78	35.66	4	4	0.172	0.150
PbTe	648608	225	2	7.89	0.80	38.51	4	4	0.213	0.169
PGa	067772	186	4	4.02	1.30	75.97	2	1	0.793	0.095
PGa	041676	216	2	4.01	1.60	76.33	3	11	1.050	0.498
PGa	635031	166	4	4.05	0.61	68.92	1	4	0.294	0.515
PCa_3N	106350	221	5	2.61	0.78	62.89	3	2	0.421	0.439
PbSe	648514	62	8	7.95	0.40	43.36	4	4	0.128	0.105
PbSe	038294	225	2	7.96	0.40	46.65	4	4	0.137	0.123
P_2K_4Be	300110	166	7	1.66	1.15	17.62	7	1	13.060	0.134
$P_2Zn_2Se_6$	413166	148	10	4.27	1.19	1.85	4	1	2.495	0.083
$P_2Se_6Cd_2$	620237	148	10	4.54	1.11	2.05	4	1	3.046	0.098
PBa_2Cl	028134	166	4	3.89	1.26	26.38	24	5	14.267	0.953
$PAsB_2$	181293	1	4	4.13	1.07	146.70	2	3	0.423	0.307
P_2ZnSi	648145	122	8	3.34	1.35	84.13	1	5	0.431	0.198
$PMnSe_3$	054140	148	10	3.99	1.72	1.72	5	4	9.964	3.081
PKS_4Ag_2	420033	121	8	3.66	1.54	29.49	5	1	0.513	0.092
$P_2S_6Rb_2$	416176	71	10	2.33	1.80	7.64	4	1	3.320	3.270
PS_3Fe	061392	12	10	2.74	1.77	4.66	9	1	5.294	2.863
PbS	068712	5	4	7.40	0.43	52.77	4	4	0.118	0.122
PbS	183250	28	8	7.37	0.45	48.43	4	4	0.127	0.121
PbS	648448	63	4	7.34	1.19	116.41	6	5	0.510	0.715
PbS	183244	194	4	7.28	0.04	22.49	1	4	0.057	0.120
PbS	183254	38	8	6.56	0.47	22.09	3	1	0.453	0.178
PbS	183255	186	4	7.11	0.50	27.96	4	3	0.796	0.213
PbS	183243	160	2	7.37	0.45	48.23	4	4	0.131	0.138
PbS	648451	62	8	7.37	0.44	52.72	4	4	0.112	0.115
PbS	183248	11	8	6.53	0.60	16.37	2	1	0.541	0.161

Energy & Environmental Science Accepted Manuscript

Compound	ICSD No.	SG No.	n	d	E_g	B	N_V	N_C	$m^*_{DOS,V}$	$m^*_{DOS,C}$
PbS	601032	225	2	7.37	0.45	52.84	4	4	0.141	0.147
PB	615154	216	2	2.95	1.26	162.04	3	6	0.503	0.796
PB	615155	186	4	2.95	1.07	162.56	2	2	0.321	0.176
PLi_3	642223	194	8	1.46	0.76	39.77	2	2	1.467	0.374
$P_2K_2S_6$	033278	71	10	1.96	1.70	8.68	4	1	2.945	2.471
P_2Fe	015027	58	6	5.17	0.72	168.74	4	2	0.502	1.475
P_4V	038315	15	10	3.29	0.19	67.51	2	1	1.753	0.512
PK_2Ag	402572	63	8	3.13	1.37	21.23	3	2	3.633	0.256
P_4Si_4Fe	079005	1	9	3.35	1.23	105.84	8	1	2.492	1.048
RuP_2	000992	58	6	6.16	0.45	181.17	6	2	0.146	1.041
RuC	183170	216	2	7.99	0.99	253.62	11	6	4.317	1.354
$RuAs_2$	611294	58	6	8.12	0.47	146.13	6	2	0.236	0.697
$RuSi_4P_4$	079006	1	9	3.66	1.52	116.39	6	2	0.843	0.465
RuSi	085209	198	8	8.20	0.36	215.04	2	3	6.318	12.646
RuGe	085211	198	8	10.00	0.26	178.20	2	3	6.050	12.339
$SBiCuCl_2$	413289	63	10	5.57	1.03	33.79	7	1	2.421	0.327
SnO_2	056676	58	6	6.62	0.66	167.16	1	1	1.337	0.030
SnO_2	056674	136	6	6.62	0.66	167.10	1	1	1.337	0.029
SSn	043409	216	2	3.63	0.14	35.14	12	3	1.397	0.911
SSn	651015	225	2	5.07	0.21	54.16	12	8	1.102	0.955
SSn	100672	63	4	5.06	0.33	23.18	2	1	0.120	0.141
SSn	651025	62	8	4.94	0.94	22.11	3	2	1.372	0.154
SbS_4Na_3	044707	217	8	2.78	1.91	21.37	17	2	2.763	0.466
$SiSe_4FeCu_2$	627368	121	8	4.99	0.78	58.93	1	0.5	0.749	0.783
SrCuSb	053339	194	6	5.69	0.01	43.92	2	3	0.117	0.599
S_2FeRb	633208	15	8	2.99	1.41	14.51	3	1	1.758	7.883
$SrMn_2P_2$	049019	164	5	3.89	0.47	56.45	2	3	0.687	1.188
Se_4BaAg_2Sn	170856	23	8	5.61	0.24	27.71	3	1	0.289	0.077
S_3TeCu_3Cl	088685	160	8	4.53	1.12	47.51	3	2	1.143	0.639
SrCuP	053323	194	6	4.80	0.09	62.00	2	3	0.190	1.176
SbS_2BrCd	171723	12	10	4.85	1.53	22.59	4	2	1.879	0.527
$SiMg_2$	150956	225	3	1.99	0.22	54.52	3	3	1.167	0.416
S_4BaAg_2Sn	041898	23	8	4.83	0.63	36.55	3	1	0.498	0.070
$SbKS_2$	060138	15	8	3.02	1.59	13.41	5	3	1.140	1.447
S_2KFe	068383	15	8	2.51	1.36	15.56	3	1	1.875	7.544
SiC	181128	216	2	3.17	1.38	213.33	3	3	1.989	0.184
SiC	028389	216	2	3.17	1.38	213.33	3	3	2.005	0.182
SiC	024261	186	4	3.17	2.37	213.92	2	2	1.487	0.420
SbMnRb	643396	129	6	4.35	1.01	18.17	2	1	2.341	0.083
Se_2Rb_2Pd	648724	71	5	4.74	1.10	24.91	7	4	3.881	2.308
SV	033613	194	4	3.99	1.78	87.40	3	2	5.695	1.020
SV	024564	62	8	4.08	1.88	84.86	6	1	2.165	0.614
S_3BaV	154182	36	10	3.88	1.39	25.74	3	3	4.512	10.209
S_3BaV	063228	63	10	3.87	1.40	25.73	3	3	4.753	10.314
S_3BaV	063230	20	10	3.88	1.39	25.73	6	3	4.703	10.281
S_2FeCu	080094	122	8	4.10	0.86	70.23	6	5	1.132	5.663
ScSbPd	415944	216	3	6.87	0.09	94.76	3	3	0.434	1.766
Se_2GaCu	247513	122	8	5.35	0.51	57.46	3	1	0.687	0.017
Se_2GaAg	605211	122	8	5.38	0.63	46.55	1	1	0.574	0.020
Sb_2SnCd	044259	122	8	5.45	0.07	36.69	3	1	0.845	0.023

Energy & Environmental Science Accepted Manuscript

This journal is © The Royal Society of Chemistry [year]

Compound	ICSD No.	SG No.	n	d	E_g	B	N_V	N_C	$m^*_{DOS,V}$	$m^*_{DOS,C}$
SeCd	415784	186	4	5.33	0.57	44.46	3	1	1.688	0.016
SeCd	620439	216	2	5.34	0.52	44.59	3	1	1.778	0.017
Se_4FeGa_2	631817	111	7	4.79	0.65	39.13	1.5	0.5	1.646	0.047
S_4CoGa_2	052961	82	7	3.62	1.56	42.51	1.5	0.5	1.617	9.122
S_4FeCu_2Sn	181166	81	8	4.37	0.23	63.20	1.5	1	0.939	0.084
S_4FeCu_2Sn	627358	121	8	4.37	0.57	62.75	1.5	1.5	0.836	0.052
SnPtTi	105799	216	3	9.92	0.72	133.89	3	3	4.235	2.284
Se_2AlAg	604704	122	8	4.78	1.52	48.93	1	1	1.997	0.036
S_4BaFe_2	023081	87	7	3.72	1.35	22.69	4	1	6.024	1.229
SiAlLi	052630	216	3	1.97	0.11	62.97	3	3	0.362	0.252
$S_4Pd_3Rb_2$	041886	12	9	4.46	1.46	17.13	7	2	4.884	2.495
$S_2Bi_2AgCl_3$	413938	12	8	5.92	1.37	35.01	2	1	3.134	0.202
$S_4Pt_3Rb_2$	026267	69	9	6.29	1.76	16.47	7	2	1.072	2.173
SrAgP	052596	194	6	5.29	0.35	50.45	2	1	0.165	0.025
$SbLi_3$	642341	225	4	3.35	0.70	32.38	4	3	1.271	0.334
$SbLi_3$	026879	194	8	2.98	0.49	28.62	2	2	1.042	0.135
S_2BiRb	052735	166	4	5.07	1.35	37.21	4	1	10.462	0.175
$ScSe_2Ag$	155115	164	4	5.68	1.24	57.02	2	3	0.568	2.253
SiB_6	020240	221	7	2.18	0.05	150.66	3	6	0.336	0.812
SbS_2Na	049016	12	8	3.56	0.81	22.82	9	2	2.142	0.677
SbS_2Na	200597	2	8	3.47	0.93	21.18	1	3	0.258	1.245
SbS_2Na	071091	15	8	3.46	0.94	21.17	1	3	0.257	1.247
SbBaAg	056981	194	6	6.27	0.08	35.03	2	3	0.110	0.438
SCd	067776	186	4	4.60	1.12	53.07	3	1	1.895	0.033
SCd	181739	216	2	4.60	1.05	53.27	3	1	1.996	0.034
SCd	108230	225	2	5.77	0.28	72.05	3	3	6.123	0.137
SbAl	024804	216	2	4.08	1.23	49.43	3	11	0.994	0.583
SbAl	052651	216	2	4.08	1.23	49.43	3	11	0.995	0.583
S_2BaCu_2	615832	139	5	5.59	0.73	62.12	1	1	0.828	0.324
S_2PdCl_6	039434	2	9	2.39	1.98	2.07	2	2	7.002	5.108
Si	030101	186	4	2.28	0.45	88.73	2	3	0.386	0.514
Si	182732	1	4	2.28	0.45	88.73	2	3	0.386	0.507
Si	060388	227	2	2.28	0.62	88.76	3	6	0.653	0.640
Si	067788	216	2	2.28	0.62	88.76	3	6	0.652	0.642
Si	181908	139	4	2.16	0.38	80.99	2	5	0.422	1.006
Si	181909	12	8	2.20	0.23	80.38	1	2	0.117	0.268
$SbKS_4Ag_2$	082143	121	8	3.96	0.82	22.03	5	1	0.645	0.102
ScS_2Cu	015298	156	4	3.80	1.50	75.15	4	3	1.964	2.170
SrP_2Li_4	416888	166	7	2.35	0.97	42.03	2	3	0.853	0.525
SbKSn	033933	186	6	4.10	0.25	20.45	2	7	0.529	0.062
S_4ZnCu_2Sn	262388	82	8	4.48	0.57	63.93	3	1	1.148	0.036
S_4ZnCu_2Sn	184478	121	8	4.48	0.43	64.72	2	1	1.308	0.035
Se	022251	152	3	4.43	1.03	4.45	11	2	2.067	0.433
SrC_2	618813	139	3	3.19	1.63	46.25	2	2	5.003	0.474
S_2Rb_2Pt	026259	71	5	5.28	1.59	30.91	5	4	3.893	2.591
Sr_3NSb	152052	221	5	4.66	0.26	45.86	3	2	0.465	0.337
Si_2W	652549	180	9	9.64	0.18	213.76	3	9	0.398	0.888
Se_4V_5	652166	87	9	5.09	1.08	44.34	1	1.5	1.399	3.723
$S_4CoSnCu_2$	099294	121	8	4.49	0.49	64.72	1.5	1.5	0.887	1.035
SbBaLi	280574	194	6	4.54	0.70	29.75	3	3	0.464	0.663

Energy & Environmental Science Accepted Manuscript

Compound	ICSD No.	SG No.	n	d	E_g	B	N_V	N_C	$m^*_{DOS,V}$	$m^*_{DOS,C}$
SZr_2N_2	096970	164	5	5.25	0.89	150.54	1	2	0.203	0.783
SZr_2N_2	096971	194	10	5.26	0.90	153.03	1	4	0.222	0.850
Se_2FeRb	040781	15	8	3.90	1.09	12.84	3	1	1.424	5.974
SrPLi	416889	194	6	3.10	1.34	44.13	3	3	0.656	0.819
SrPLi	056443	187	3	3.06	0.80	42.41	3	3	0.868	1.485
STe_2Bi_2	026720	148	5	7.14	0.37	7.58	1	1	0.098	0.033
Sb_2Mn_2Sr	041790	164	5	4.98	0.52	39.77	2	3	0.592	1.267
Se_2AlCu	600586	122	8	4.63	1.41	60.06	1	1	0.865	0.030
SbZnLi	042064	186	6	5.17	0.38	45.84	1	1	0.438	0.066
$SiTe_4Cu_2Cd$	656151	121	8	5.61	0.56	44.96	3	1	0.948	0.024
S_4GeCu_2Fe	627306	121	8	4.17	0.74	68.26	1.5	0.5	0.803	0.734
ScNiSb	040296	216	3	6.42	0.04	99.11	3	3	0.545	1.608
ScNiSb	076695	216	3	6.42	0.04	99.11	3	3	0.544	1.609
SnSe	076032	225	2	5.97	0.19	48.47	12	8	0.767	0.594
SnSe	651925	63	4	5.99	0.31	22.96	4	1	0.151	0.193
SnSe	071338	39	4	5.92	0.13	48.40	12	8	0.566	0.358
SnSe	050557	62	8	5.86	0.61	21.87	2	3	0.395	0.114
$S_4Br_2Bi_3Ag$	413939	12	10	6.03	0.73	15.41	1	1	0.335	0.420
SbS_2MnBr	172782	12	10	4.40	1.39	26.29	2	1	1.633	0.571
SeV	162898	129	4	5.34	1.46	70.76	8	1	2.774	0.873
SeV	652164	194	4	5.41	1.85	72.89	2	2	4.828	1.170
SPt	654379	131	4	9.93	0.91	117.96	6	1	2.514	0.713
Se_2CuIn	154409	122	8	5.50	0.10	50.55	3	1	1.534	0.012
SiCGaN	183047	31	8	4.57	0.57	120.81	3	1	0.692	0.169
SiGaLi	103786	216	3	3.43	0.18	58.95	3	3	0.263	0.503
SeIn	041477	160	4	4.92	0.66	2.14	1	1	0.818	0.037
Te_2Rb_2Pt	649525	71	5	5.72	1.07	20.09	6	4	2.387	1.394
TeSn	652742	225	2	6.25	0.02	39.93	4	4	0.041	0.109
TeSn	053956	216	2	4.38	0.05	24.58	12	3	0.847	1.122
Te_2AlAg	028746	122	8	5.12	1.32	39.02	1	1	0.605	0.034
Te_2LiIn	658016	122	8	4.60	1.40	23.40	3	1	0.920	0.090
Te_2BiAg	043266	166	4	7.90	0.17	43.03	10	5	0.817	0.117
Te_3Bi_2	184631	166	5	7.32	0.51	10.96	1	1	0.471	0.066
Te_2AgIn	605476	122	8	5.63	0.34	33.64	3	1	0.603	0.016
TeHg	639251	154	6	8.23	0.52	12.12	1	1	0.580	0.237
TeHg	041593	152	6	8.23	0.50	12.10	1	1	0.558	0.235
Te_4Cu_3V	629351	215	8	5.82	0.73	24.43	3	3	1.035	2.144
TeCd	620518	186	4	5.50	0.63	34.78	3	1	1.261	0.015
TeCd	043712	216	2	5.50	0.60	35.00	3	1	1.424	0.017
TeCd	067862	152	6	6.18	0.03	36.59	1	1	0.747	0.009
TeBiCl	079362	186	6	5.76	1.37	2.86	2	1	2.078	0.119
Te_2AlCu	028735	122	8	5.09	1.36	47.03	3	1	0.736	0.032
Te_2GaLi	162673	122	8	4.47	1.60	26.78	1	5	0.516	0.126
YTe_2Ag	605920	113	8	6.01	1.13	38.70	1	2	0.254	0.697
$ZnAs_2Si$	023707	122	8	4.54	0.90	66.84	1	1	0.372	0.023
ZnAsLi	074504	216	3	4.59	0.56	53.85	3	1	0.722	0.014
ZnSe	652222	216	2	5.07	1.17	56.44	3	1	1.557	0.021
ZnSe	067778	186	4	5.07	1.21	56.17	3	1	1.342	0.020
ZnSe	162905	129	4	4.49	2.02	1.36	3	2	2.471	0.393
ZnS_4GeCu_2	627794	121	8	4.29	0.80	69.64	2	1	1.197	0.045

Energy & Environmental Science Accepted Manuscript

Compound	ICSD No.	SG No.	n	d	E_g	B	N_V	N_C	$m^*_{DOS,V}$	$m^*_{DOS,C}$
ZnLiN	016790	216	3	4.78	0.52	112.40	3	1	1.956	0.023
$ZnTe_4SiCu_2$	656150	121	8	5.54	0.40	47.62	2	3	0.745	0.088
ZnO	163383	216	2	5.45	0.63	128.80	3	1	3.457	0.031
ZnO	182359	225	2	6.63	0.73	165.85	2	1	7.264	0.030
ZnO	076641	186	4	5.45	0.73	128.62	3	1	2.801	0.031
ZnTe	104196	216	2	5.43	1.08	43.21	3	1	1.228	0.020
ZnTe	067779	186	4	5.42	1.11	42.90	3	1	1.028	0.019
ZnTe	080076	144	6	5.42	1.07	43.19	3	1	1.077	0.019
ZnTe	184487	152	6	6.01	0.27	47.10	1	1	0.547	0.011
ZrSnPd	105705	216	3	7.50	0.09	89.57	3	8	3.075	1.580

References

1 V. W. L. Chin, T. L. Tansley and T. Osotchan, J. Appl. Phys., 1994, **75**, 7365–7372.
2 J. Edwards, K. Kawabe, G. Stevens and R. Tredgold, Solid State Comm., 1965, **3**, 99–100.
3 R. J. Stirn and W. M. Becker, Phys. Rev., 1966, **148**, 907–919.
4 R. J. Stirn and W. M. Becker, Phys. Rev., 1966, **141**, 621–628.
5 W. P. Allred, W. L. Mefferd and R. K. Willardson, J. Electrochem. Soc., 1960, **107**, 117–122.
6 F. J. Ried and R. K. Willardson, J. Electron. Control, 1958, **5**, 54–61.
7 M. Iwami, T. Tohda and K. Kawabe, Elec. Eng. Japan, 1975, **95**, 19–24.
8 N. Kato, W. Kammura, M. Iwami and K. Kawabe, Jpn. J. Appl. Phys., 1977, **16**, 1623–1627.
9 B. Stone and D. Hill, Phys. Rev. Lett., 1960, **4**, 282–284.
10 F. Nava, C. Canali, C. Jacoboni, L. Reggiani and S. Kozlov, Solid State Comm., 1980, **33**, 475 – 477.
11 A. G. Redfield, Phys. Rev., 1954, **94**, 526–537.
12 L. Reggiani, S. Bosi, C. Canali, F. Nava and S. F. Kozlov, Phys. Rev. B, 1981, **23**, 3050–3057.
13 P. T. Wedepohl, Proc. Phys. Soc. Sec. B, 1957, **70**, 177.
14 W. G. Zeier, A. Zevalkink, E. Schechtel, W. Tremel and G. J. Snyder, J. Mater. Chem., 2012, **22**, 9826–9830.
15 E. S. Toberer, A. Zevalkink, N. Crisosto and G. J. Snyder, Adv. Funct. Mat., 2010, **20**, 4375–4380.
16 A. Zevalkink, J. Swallow and G. J. Snyder, Dalton Trans., 2013, **42**, 9713–9719.
17 A. Zevalkink, G. S. Pomrehn, S. Johnson, J. Swallow, Z. M. Gibbs and G. J. Snyder, Chem. Mater., 2012, **24**, 2091–2098.
18 F. A. Kroger, H. J. Vink and J. Volger, Phillips Res. Rep., 1955, **10**, 39.
19 M. Islam and J. Woods, Solid State Comm., 1969, **7**, 1457 – 1461.
20 J. Mort and W. E. Spear, Phys. Rev. Lett., 1962, **8**, 314–315.
21 M. Onuki and N. Hase, J. Phys. Soc. Japan, 1965, **20**, 171–171.
22 D. M. Heinz and E. Banks, J. Chem. Phys., 1956, **24**, 391–398.
23 M. Itakura and H. Toyoda, Jpn. J. Appl. Phys., 1965, **4**, 560.
24 W. Gloede, H. Lippmann and S. Mutze, Phys. Stat. Solidi A, 1971, **6**, K69–K71.
25 Z. R. Baubinas, A. Janukevi?ius and J. V. Sakalas, Solid State Comm., 1974, **15**, 1731–1733.
26 A. D. Petravichyus, G. B. Yushka and R. V. Baubinas, Sov. Phys. Semicond., 1976, **9**, 54.
27 R. Triboulet and Y. Marfaing, J. Electrochem. Soc., 1973, **120**, 1260–1265.
28 V. D. Popovych, I. S. Virt, D. I. Tsutsura, Z. F. Tsybrii, F. F. Sizov, O. A. Parfenjuk and M. I. Ilashchuk, Phys. Stat. Solidi C, 2006, **3**, 717–721.
29 J. W. Sharp, E. C. Jones, R. K. Williams, P. M. Martin and B. C. Sales, J. Appl. Phys., 1995, **78**, 1013–1018.
30 T. Caillat, A. Borshchevsky and J. P. Fleurial, AIP Conference Proceedings, 1994, **316**, 58–61.
31 Y. Nagamoto, K. Tanaka and T. Koyanagi, Proc. Int. Conf. Thermoelectrics, 1998, **17**, 302–305.
32 X. Y. Li, L. D. Chen, J. F. Fan, W. B. Zhang, T. Kawahara and T. Hirai, J. Appl. Phys., 2005, **98**, 083702.
33 H. Anno, K. Matsubara, Y. Notohara, T. Sakakibara and H. Tashiro, J. Appl. Phys., 1999, **86**, 3780–3786.
34 E. Arushanov, K. Fess, W. Kaefer, C. Kloc and E. Bucher, Phys. Rev. B, 1997, **56**, 1911–1917.
35 G. J. Wang and F. L. Weichman, Canada J. Phys., 1982, **60**, 1648–1655.
36 M. Zouaghi, M. Tapiero, J. Zielinger and R. Burgraf, Solid State Comm., 1970, **8**, 1823 – 1825.
37 H. McKinzie and M. O'Keeffe, Phys. Lett. A, 1967, **24**, 137 – 139.
38 J. Tate, H. L. Ju, J. C. Moon, A. Zakutayev, A. P. Richard, J. Russell and D. H. McIntyre, Phys. Rev. B, 2009, **80**, 165206.
39 K. Irmscher, Z. Galazka, M. Pietsch, R. Uecker and R. Fornari, J. Appl. Phys., 2011, **110**, 063720.
40 P. Blood, Phys. Rev. B, 1972, **6**, 2257–2261.
41 H. Hicks and D. Manley, Solid State Comm., 1969, **7**, 1463–1465.
42 H. Miki and M. Otsubo, Jpn. J Appl Phys, 1971, **10**, 509.

Energy & Environmental Science Accepted Manuscript

43 D. E. Hill, J Appl Phys, 1970, **41**, 1815–1818.
44 A. L. Mears and R. A. Stradling, J. Phys. C: Solid State Phys., 1971, **4**, L22.
45 M. Toyama, M. Naito and A. Kasami, Jpn.. J. Appl. Phys., 1969, **8**, 358.
46 R. Taylor, J. Woods and M. Lorenz, J. Appl. Phys., 1968, **39**, 5404–5411.
47 Y. Kao and O. Eknoyan, J. Appl. Phys., 1983, **54**, 2468–2471.
48 Y. Kokubun, S. Washizuka, J. Ushizawa, M. Watanabe and T. Fukuda, Appl. Phys. Lett., 1982, **41**, 841–843.
49 H. Casey Jr, F. Ermanis and K. Wolfstirn, J. Appl. Phys., 1969, **40**, 2945–2958.
50 V. V. Galavanov and N. V. Siukaev, Phys. Stat. Solidi B, 1970, **38**, 523–530.
51 L. D. Zhu, K. T. Chan and J. M. Ballantyne, Appl. Phys. Lett., 1985, **47**, 47–48.
52 M. Glicksman and K. Weiser, J. Phys. Chem. Solids, 1959, **10**, 337–340.
53 M. Benzaquen, B. Belache, C. Blaauw and R. A. Bruce, J. Appl. Phys., 1990, **68**, 1694–1701.
54 P. Li, S. Lee and G. Danielson, Phys. Rev. B, 1972, **6**, 442.
55 R. D. Redin, R. Morris and G. Danielson, Phys. Rev., 1958, **109**, 1916.
56 S. K. Bux, M. T. Yeung, E. S. Toberer, G. J. Snyder, R. B. Kaner and J.-P. Fleurial, J. Mater. Chem., 2011, **21**, 12259–12266.
57 M. Akasaka, T. Iida, A. Matsumoto, K. Yamanaka, Y. Takanashi, T. Imai and N. Hamada, J. Appl. Phys., 2008, **104**, 013703.
58 J.-Y. Jung, K.-H. Park and I.-H. Kim, IOP Conference Series: Materials Science and Engineering, 2011, p. 142006.
59 N. Farahi, M. VanZant, J. Zhao, S. T. John, S. Prabhudev, G. A. Botton, J. R. Salvador, F. Borondics, Z. Liu and H. Kleinke, Dalton Trans., 2014, 14983–14991.
60 K. Kambe and H. Udono, J. Elect. Mater., 2014, **43**, 2212–2217.
61 M. Heller and G. Danielson, J. Phys. Chem. Sol., 1962, **23**, 601–610.
62 H. Ihou-Mouko, C. Mercier, J. Tobola, G. Pont and H. Scherrer, J. All. Comp., 2011, **509**, 6503 – 6508.
63 H. Wang, E. Schechtel, Y. Pei and G. J. Snyder, Adv. Energy Mater., 2013, **3**, 488–495.
64 J. N. Zemel, J. D. Jensen and R. B. Schoolar, Phys. Rev., 1965, **140**, A330.
65 R. S. Allgaier and W. W. Scanlon, Phys. Rev., 1958, **111**, 1029.
66 L.-D. Zhao, J. He, C.-I. Wu, T. P. Hogan, X. Zhou, C. Uher, V. P. Dravid and M. G. Kanatzidis, J. Am. Chem. Soc, 2012, **134**, 7902–7912.
67 L.-D. Zhao, J. He, S. Hao, C.-I. Wu, T. P. Hogan, C. Wolverton, V. P. Dravid and M. G. Kanatzidis, J. Amer. Chem. Soc., 2012, **134**, 16327–16336.
68 H. Wang, Y. Pei, A. D. LaLonde and G. J. Snyder, Proc. Nat. Acad. Sci., 2012, **109**, 9705–9709.
69 J. Androulakis, Y. Lee, I. Todorov, D.-Y. Chung and M. Kanatzidis, Phys. Rev. B, 2011, **83**, 195209.
70 H. Wang, Y. Pei, A. D. LaLonde and G. J. Snyder, Adv. Mater., 2011, **23**, 1366–1370.
71 S. Wang, G. Zheng, T. Luo, X. She, H. Li and X. Tang, J. Phys. D: Appl. Phys., 2011, **44**, 475304.
72 U. Schlichting and K. Gobrecht, J. Phys. Chem. Sol., 1973, **34**, 753–758.
73 Y. Pei, A. LaLonde, S. Iwanaga and G. J. Snyder, Energy Environ. Sci., 2011, **4**, 2085–2089.
74 Y. Pei, A. D. LaLonde, H. Wang and G. J. Snyder, Energy Environ. Sci., 2012, **5**, 7963–7969.
75 Y. Pei, Z. M. Gibbs, B. Balke, W. G. Zeier and G. J. Snyder, Adv. Energy Mater., 2014, 1614–6840.
76 A. D. LaLonde, Y. Pei and G. J. Snyder, Energy Environ. Sci., 2011, **4**, 2090–2096.
77 F. J. Morin and J. P. Maita, Phys. Rev., 1954, **96**, 28–35.
78 C. Jacoboni, C. Canali, G. Ottaviani and A. A. Quaranta, Solid State Electron., 1977, **20**, 77–89.
79 S. S. Li and W. R. Thurber, Solid State Electron., 1977, **20**, 609–616.
80 P. Norton, T. Braggins and H. Levinstein, Phys. Rev. B, 1973, **8**, 5632–5653.
81 J. Dorkel and P. Leturcq, Solid State Electron., 1981, **24**, 821–825.
82 R. A. Logan and A. J. Peters, J. Appl. Phys., 1960, **31**, 122–124.
83 A. Suzuki, A. Uemoto, M. Shigeta, K. Furukawa and S. Nakajima, Appl. Phys. Lett., 1986, **49**, 450–452.
84 S. Nishino, J. A. Powell and H. A. Will, Appl. Phys. Lett., 1983, **42**, 460–462.
85 W. Nelson, F. Halden and A. Rosengreen, J. Appl. Phys., 1966, **37**, 333–336.
86 M. Yamanaka, H. Daimon, E. Sakuma, S. Misawa and S. Yoshida, J. Appl. Phys., 1987, **61**, 599–603.
87 M. Shinohara, M. Yamanaka, H. Daimon, E. Sakuma, H. Okumura, S. Misawa, K. Endo and S. Yoshida, Jpn.. J. Appl. Phys., 1988, **27**, L434.
88 C. G. Fonstad and R. H. Rediker, J. Appl. Phys., 1971, **42**, 2911–2918.
89 M. Zhou, Z. M. Gibbs, H. Wang, Y. Han, C. Xin, L. Li and G. J. Snyder, Phys. Chem. Chem. Phys., 2014, **16**, 20741–20748.
90 J. Kafalas, R. Brebrick and A. Strauss, Appl. Phys. Lett., 1964, **4**, 93–94.
91 R. Moos, W. Menesklou and K. H. Hardtl, Appl. Phys. A - Mater., 1995, **61**, 389–395.
92 L. Forro, O. Chauvet, D. Emin, L. Zuppiroli, H. Berger and F. Lvy, J. Appl. Phys., 1994, **75**, 633–635.
93 D. Look, D. Reynolds, J. Sizelove, R. Jones, C. Litton, G. Cantwell and W. Harsch, Solid State Comm., 1998, **105**, 399 – 401.
94 P. Wagner and R. Helbig, J. Phys. Chem. Solids, 1974, **35**, 327 – 335.
95 S. Fujita, H. Mimoto, H. Takebe and T. Noguchi, J. Cryst. Growth, 1979, **47**, 326–334.
96 S. Iida, T. Yatabe, H. Kinto and M. Shinohara, J. Cryst. Growth, 1990, **101**, 141 – 146.
97 S. Iida, T. Yatabe and H. Kinto, Jpn. J. Appl. Phys., 1989, **28**, L535.
98 I. Kikuma, M. Matsuo and T. Komuro, Jpn.. J. Appl. Phys., 1992, **31**, L531.

Energy & Environmental Science Accepted Manuscript

This journal is © The Royal Society of Chemistry [year]

99 N. D. Nedeoglo, V. Sirkeli, D. Nedeoglo, R. Laiho and E. Lähderanta, J. Phys.: Cond. Mat., 2006, **18**, 8113.
100 A. Avdonin, D. Nedeoglo, N. Nedeoglo and V. Sirkeli, Phys. Stat. Sol. B, 2003, **238**, 45–53.
101 H. Ruda, J. Appl. Phys., 1986, **59**, 1220–1231.
102 P. Lemasson, A. Riviere, G. Didier, A. Tromson-Carli and R. Triboulet, J. Cryst. Growth, 1999, **197**, 462–465.
103 H. H. Farrell, M. C. Tamargo, T. J. Gmitter, A. L. Weaver and D. E. Aspnes, J. Appl. Phys., 1991, **70**, 1033–1035.
104 A. Ohki, N. Shibata, K. Ando and A. Katsui, J. Cryst. Growth, 1988, **93**, 692–696.
105 A. G. Fischer, J. N. Carides and J. Dresner, Sol. St. Comm., 1964, **2**, 157–159.
106 S. Bhunia and D. Bose, J. Cryst. Growth, 1998, **186**, 535–542.
107 A. A. El-Soud, F. El Akkad, S. Hammad and N. Ali, J. Mater. Sci.: Mater. Electr., 1991, **2**, 171–173.
108 D. R. Lide, CRC handbook of chemistry and physics, CRC press, 2004.
109 S. A. Aliev, A. Y. Nashelskii and S. S. Shalyt, Sov. Phys. Sol. St., 1965, **7**, 1287.
110 D. T. Morelli and G. A. Slack, in High Thermal Conductivity Materials, ed. S. Shinde and J. Goela, Springer: New York, NY, 2005, ch. High lattice thermal conductivity solids, pp. 37–64.
111 G. A. Slack, R. A. Tanzilli, R. O. Pohl and J. W. Vandersande, J. Phys. Chem. Solids., 1987, **48**, 641–647.
112 T. Takahashi and T. Kikuchi, J. Nucl. Mater., 1980, **91**, 93–102.
113 L. Garbato and A. Rucci, Chem. Phys. Lett., 1979, **61**, 542 – 544.
114 G. A. Slack, Solid State Physics, Academic Press, New York, 1979, vol. 34.
115 N. A. Surplice and R. P. Jones, Brit. J. Appl. Phys., 1963, **14**, 720.
116 G. P. Akishin, S. K. Turnaev, V. Y. Vaispapir, M. A. Gorbunova, Y. N. Makurin, V. S. Kiiko and A. L. Ivanovskii, Refract. Ind. Ceram., 2009, **50**, 465–468.
117 A. J. Slifka, B. J. Filla and J. M. Phelps, J. Res. Natl. Inst. Stan., 1998, **103**, 357–363.
118 G. A. Slack and R. Newman, Phys. Rev. Lett., 1958, **1**, 359–360.
119 R. Berman, P. R. W. Hudson and M. Martinez, J. Phys. C: Sol. St. Phys., 1975, **8**, L430.
120 A. Zevalkink, E. S. Toberer, W. Zeier, E. Flage-Larsen and G. J. Snyder, Energy Environ. Science, 2011, **4**, 510–518.
121 J. G. Li, T. Ikegami and T. Mori, J. Mater. Res., 2003, **18**, 1816–1822.
122 S. Materials, Landolt – Börnstein Database, http://www.springermaterials.com/docs/index.html.
123 C. J. Glassbrenner and G. A. Slack, Phys. Rev., 1964, **134**, A1058–A1069.
124 G. Y., L. M. E. and R. S. L., in Properties of Advanced SemiconductorMaterials GaN, AlN, SiC, BN, SiC, SiGe, ed. L. M. E., R. S. L. and S. M. S., John Wiley & Sons, Inc., New York, 2001, pp. 93–148.
125 D. P. Spitzer, J. Phys. Chem. Sol., 1970, **31**, 19.
126 P. Turkes, C. Pluntke and R. Helbig, J. Phys. C: Sol. St., 1980, **13**, 4941–4951.
127 D. Morelli, T. Caillat, J. Fleurial, A. Borshchevsky, J. Vandersande, B. Chen and C. Uher, Phys. Rev. B, 1995, **51**, 9622–9628.
128 T. F. Smith, J. A. Birch and J. G. Collins, J. Phys. C: Sol. St. Phys., 1976, **9**, 4375.
129 M. Massot, A. Oleaga, A. Salazar, D. Prabhakaran, M. Martin, P. Berthet and G. Dhalenne, Phys. Rev. B, 2008, **77**, 134438.
130 M. Marinelli, F. Mercuri, U. Zammit, R. Pizzoferrato and F. Scudieri, Phys. Rev. B, 1994, **49**, 4356–4359.
131 N. Tinh and T. Tsuji, in Physics and Engineering of New Materials, ed. D. Cat, A. Pucci and K. Wandelt, Springer Berlin Heidelberg, 2009, vol. 127, pp. 209–217.
132 H. Timm and J. Janek, Sol. St. Ion., 2005, **176**, 1131–1143.
133 J. K. Chen, X. L. Liu, X. Yuan, Y. L. Zhang, Y. F. Gao, Y. F. Zhou, R. H. Liu, L. D. Chen and N. F. Chen, Chinese Sci. Bull., 2012, **57**, 3393–3396.
134 S. Yanagiya, N. V. Nong, J. X. Xu and N. Pryds, Materials, 2010, **3**, 318–328.
135 E. Takegoshi, Y. Hirasawa, S. Imura and T. Shimazaki, Inter. J. Thermophy., 1984, **5**, 219–228.
136 E. G. Villora, K. Shimamura, T. Ujiie and K. Aoki, Appl. Phys. Lett., 2008, **92**, 202118.
137 R. O. Carlson, G. A. Slack and S. J. Silverman, J. Appl. Phys., 1965, **36**, 505–507.
138 V. M. Muzhdaba, A. Y. Nashelskii, P. V. Tamarin and S. S. Shalyt, Sov. Phys. Sol. St., 1968, **10**, 2265–2267.

Energy & Environmental Science Accepted Manuscript

This journal is © The Royal Society of Chemistry [year]

We develop a semi-empirical model for thermoelectric performance and demonstrate its utility for high throughput computational searches.

Energy & Environmental Science Accepted Manuscript